NAZARBAYEV UNIVERSITY

School of Engineering and Digital Sciences

Bachelor of Engineering in

Mechanical and Aerospace Engineering

Study of mechanical behavior of novel fiber metal laminates

(Final Capstone Project Report)

by

Sadyr Sabitov, Margarita Kashirina, and Nurgul Abdiashim

Lead Supervisor: Prof. Gulnur Kalimuldina

Co-Supervisors: Prof. Sherif A. Gouda, Dr. Umut Bakhbergen

April, 2024

Declaration

We, Sadyr Sabitov, Margarita Kashirina, and Nurgul Abdiashim, hereby declare that this report, entitled “Study of mechanical behavior of novel fiber metal laminates” is the result of our own project work except for quotations and citations which have been duly acknowledged. We also declare that it has not been previously or concurrently submitted for any other degree at Nazarbayev University or elsewhere.

Signature: 

Name: Sadyr Sabitov

Date: April 28, 2024

Signature: 

Name: Nurgul Abdiashim

Date: April 28, 2024

Signature: 

Name: Margarita Kashirina

Date: April 28, 2024

Acknowledgements

We would like to express our sincere gratitude to our supervisors, Prof. Gulnur Kalimuldina and Prof. Sherif A. Gouda, for their guidance and support throughout this project. Special thanks Dr. Umut Bakhbergen for her support, patience and guidance. We would also like to thank Prof. Didier Talamona and Prof. Asma Perveen for providing access to laboratory equipment.

Abstract

FMLs are a class of advanced hybrid materials, constructed by alternately bonding layers of metal with layers of fiber-reinforced polymers, providing the enhanced mechanical properties of all components. The advantages of this composite material include high strength-to-weight ratio, fatigue, and damage resistance, making it well-suited for aircraft construction. However, one of the main challenges related to the FML structures is interfacial delamination, which becomes a reason for early failures. This research investigates the ways to improve the interfacial strength between the composite's layers by studying: the effect of cellulose nanofibers on the tensile strength and Young's modulus of polyurethane experimentally; the effect of nanomaterial on the shear strength of single-lap joints – both experimentally and numerically; the effect of mechanical and chemical treatment on the shear strength of single-lap joints; the synergetic effect of CNF and surface treatment on the shear strength.

The study reveals that the addition of CNF can significantly enhance the tensile strength of the polymer and the shear strength of the adhesive joints but only up to a certain limit. 1 wt% of CNF increased the tensile strength and Young's modulus of the polymer by 401% and 66.6% respectively, while for the single-lap joints, the highest shear strength was achieved with 0.5 wt% of CNF giving an 86% increase. It was also investigated that both mechanical and chemical treatment considerably improve the bonding strength in the single-lap joints, and the best result can be achieved by the synergy of chemical treatment and the addition of CNF, which improves the shear strength by 137%. The obtained numerical results for the single-lap shear test from the computer simulation are close to the experimental values and can be used for further investigation of single-lap joints' mechanical behavior. The findings of this study may provide valuable insights into the development of next-generation FMLs with improved performance and durability.

Contents

List of Figures

List of Tables

1. Introduction

In today's industry and engineering fields, material trends are shaped by an increasing need for enhanced mechanical properties, design flexibility, and cost-effectiveness. This demand is influenced by challenges arising from rapid technological development, the drive for efficiency and optimal resource utilization, regulatory requirements, and an increased awareness of environmental concerns. One of the solutions to relevant issues in manufacturing is the usage of innovative composite materials, which combine characteristics of two or more materials, providing enhanced properties of all components. A vivid example of such materials is Fiber Metal Laminates (FMLs) - a unique blend of metal sheets and fiber-reinforced composites, offering a solution to the limitations of traditional materials used in aircraft construction. For example, as presented in Figure 1.1, Glass laminate aluminum reinforced epoxy (GLARE) is used to construct the upper fuselage and leading edges of the Airbus A380 preventing crack propagation and providing higher residual strength and impact resistance.

Figure 1.1. GLARE deployment in the Airbus A380 [1].

These laminates are created by bonding layers of metals like aluminum or titanium with fiber-reinforced polymers such as fiberglass or carbon fiber-reinforced polymers (CFRP) as presented in Figure 1.2.

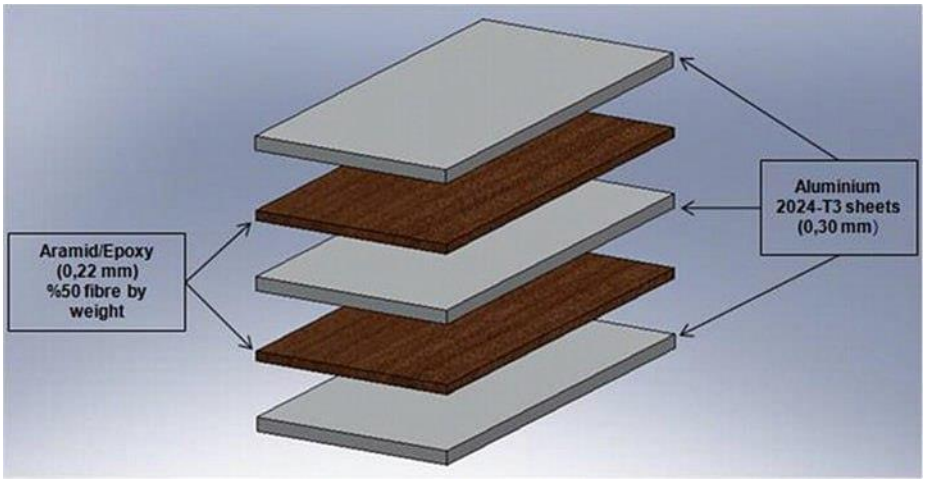

Figure 1.2. FML structure [2].

The primary objective of developing these laminates was to address the disadvantages of monolithic metal and fiber-reinforced composites when they are used separately. While monolithic aluminum and its alloys exhibit poor fatigue strength, fiber-reinforced composites lack impact resistance [2, 3]. Modern FMLs, such as glass-reinforced laminate (GLARE), surpass both aluminum alloys and CFRPs in their high strength-to-weight ratio, fatigue, and damage resistance [3, 4]. The performance of these laminates is significantly influenced by the bonding strength between the polymer and metal and by the strength properties of the polymer itself [4]. Common strategies to enhance the strength of the interface between metal and polymer include improving the surface of the metal through acid etching, anodizing, or mechanically altering the surface roughness [4]. The reason behind this is the formation of surface oxide layers containing microscale pits providing deep penetration of the polymer resin to the surface leading to a strong interfacial bonding by mechanical interlocking mechanism [5]. Nowadays, another innovative strategy involving the addition of nanofibers to the polymer is getting more popular. Unlike such methods as surface treatment, the addition of nanoparticles also improves several properties of polymers including thermal stability, storage modulus, and loss modulus [6]. Nanofibers, categorized based on the raw material into organic, inorganic, carbon, and composite fibers have gained significant attention in recent years [5]. They can be produced using various methods, making them suitable for almost any tissue engineering process with appropriate modifications. According to Eslami-Farsani [5], starting in 2018 the number of published articles about the application of nanoparticles in FML production has increased 3 times compared to the mid-2010s, and

the most commonly used type is carbon nanotubes (CNTs). The reason for this is that CNTs can increase the adhesion by more than 40% without chemically affecting the metal.

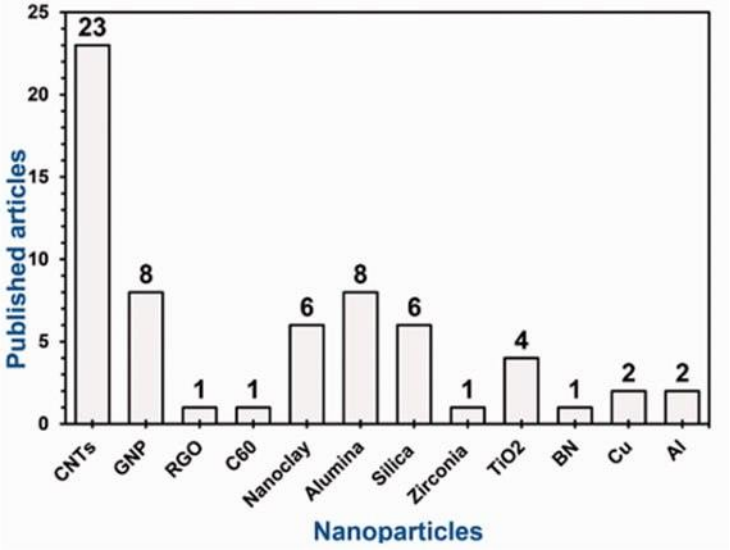

Figure 1.3. Number of related articles on the effect of FMLs containing nanoparticles [5].

It is important to notice that the addition of nanoparticles has a positive impact on the strength of FMLs only up to a certain concentration followed by significant deterioration of properties with further increase of particle content [7]. Also, the production of carbon nanoparticles requires quite a lot of resources, such as energy, specialized equipment, and raw materials, because the synthesis of CNTs includes electric-arc discharge, laser ablation, or chemical vapor deposition [8]. Therefore, the need for other more environmentally friendly and cost-advantageous options appears. Cellulose nanofibers (CNF), a type of natural nanofiber, have been recognized for their exceptional properties such as biocompatibility, degradability, stiffness, surface energy, enhanced surface reactivity, strong entangled nano-porous networks, enhanced water absorptivity and swelling, and high thermal and electrical conductivity [9]. Moreover, CNF may be produced using more available and simple ways in comparison to CNTs, such as oxidation, enzymatic hydrolysis, cationization, or even fully mechanical methods [10]. They also possess a beneficial surface area-to-volume ratio, high crystallinity, high mechanical strength, and low density.

This research aims to study the ways to increase the interface strength of the aluminum-polyurethane adhesive joints for FML applications. The hypothesis of the research

is that the addition of cellulose nanofibers to the adhesive and roughening of the metal surface can improve the adhesive strength of aluminum-polyurethane (Al-PU) joints, and their behavior can be modeled in computer simulation software. For this reason, the following objectives are set:

- to study the effect of cellulose nanofibers on the tensile strength of the polymer and single-lap shear strength of the adhesive joints;
- to study the effect of mechanical and chemical surface treatment on the single-lap-shear strength;
- to study the synergetic effect of surface treatment and addition of nanofibers on the single-lap shear strength;
- to model the behavior of adhesive joints in the single-lap shear strength test.

Table 1.1. Team Composition & Distribution of Tasks

Team member	**Task description**
Sadyr Sabitov	Literature review, preparation of single-lap joints and polyurethane samples, testing, preparation of mechanically treated samples, data analysis
Nurgul Abdiashim	Literature review, computer modeling in the Abaqus software, finding data for mode 1 and mode 2 from existing research, data analysis
Margarita Kashirina	Literature review, preparation of single-lap joints and polyurethane samples, preparation of chemically treated samples, testing, data analysis

Current research focuses on the highly developed carbon-based nanomaterial, while this study will be focused on the natural nanofibers – CNF. As nowadays sustainability has become one of the key factors affecting material production, this option has a great potential to substitute other nanomaterials in the reinforcement of FMLs. In addition, even though the effect of surface treatment has been already deeply studied, there is limited research on the

synergetic effect of nanofibers combined with different types of surface treatment, which will be discussed in this paper. For the experimental testing, it was decided to use a single-lap shear test. The single-lap shear test is one of the oldest methods to identify the shear strength of adhesive materials [11]. This test is not only known for wide research but also is proven to produce large amounts of peel stress, which would help to identify the maximum shear strength of the adhesive [12]. One of the reasons to use a single lap shear test is that this test is easy to perform and can be carried out through mixed mode loading [13]. One of the software that can be used to create and examine mechanical parts and assemblies, and for the visualization of the outcomes of finite element analysis is the Abaqus FEA software suite. It is considered user-friendly software, which can solve complex problems. This combination of characteristics makes it suitable to use in this study. The findings of this study could contribute to the development of next-generation FMLs with superior performance and durability.

2. Literature review

One of the main challenges related to the FML structures is interfacial delamination, and according to many experimental studies, it causes early failures [14]. Figure 1.4 demonstrates a lateral view of delamination occurrence on the FML structure layer. The delamination process mainly happens under different types of loading. According to M. Kamocka and R. J. Mania [15], delamination growth happens due to fatigue, shear, and impact loading. Delamination occurs when the energy release rate or delamination driving force is more than the delamination resistance of the interface [15]. However, in recent research, the main cause of delamination buckling behavior was pulse loading, which was identified through Finite Element Modeling [16].

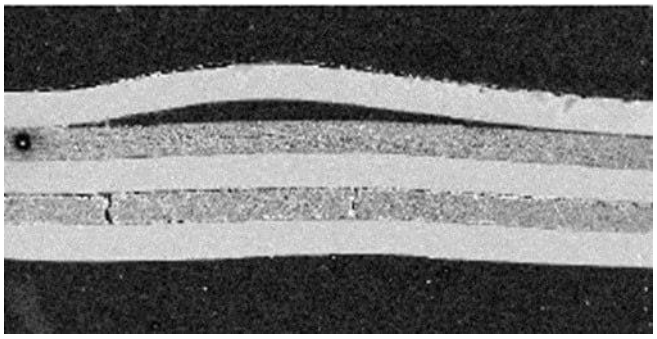

Figure 1.4. Lateral view cut of a FML with delamination buckling [17].

Therefore, several solutions were suggested to deal with delamination problems, such as addition of nanomaterials and surface treatment. Over the past decade, nanoparticles have gained significant attention due to their ability to enhance the mechanical properties of composite materials. There is a wide range of nanoparticles commonly integrated into FMLs including carbon nanotubes, graphene, nanoclays, metal, and silica nanoparticles, contributing to improved mechanical strength, thermal conductivity, and overall performance. According to Kamocka and Mania [15], the reason behind the improvement of the adhesive's strength is the blocking of crack propagation when the load is transferred through a matrix to fibers. Moreover, there are several toughening mechanisms provided by the nanofibers during crack propagation. According to Mahato et al. [18], the most common mechanisms are nanofiber bridging, crack deflection, and crack arrest. As presented in Figure 1.5 (a), nanofiber bridging is a phenomenon when a fiber holds laminae together at the place

of crack and delays its propagation. Figure 1.5 (b) shows crack deflection when the crack changes its direction along the fiber. This process consumes the energy brought by the crack, and therefore, improves the toughness of a material. The last process, illustrated in Figure 1.5 (c), does not allow microcracks to propagate further as their sizes are less than the size of a fiber.

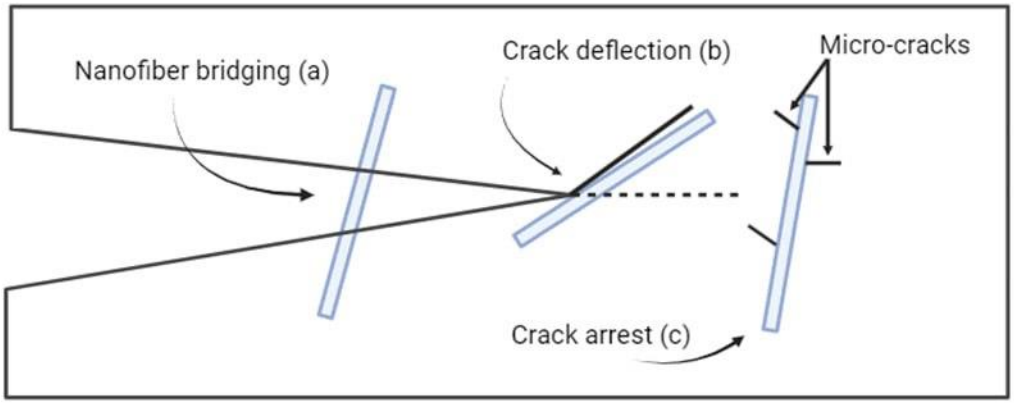

Figure 1.5. Schematic diagram of the toughening mechanisms [18].

In the study of Megahed et al. [19], the ability of different nanofillers to enhance the mechanical properties of GLARE fiber-metal laminate was explored. The nanomaterials presented in the research are aluminum (Al), copper (Cu), titanium oxide (TiO_2), silica (SiO_2), aluminum oxide (Al_2O_3), and nanoclay (NC) and they all were taken in 1 wt%. The highest ultimate tensile strength of nanofiber metal laminates was present in the SiO_2/Glare FMLs. Multiple studies have examined not only the effect of different types of nanoparticles on the properties of composite materials but also the effect of their dosage in the adhesive. For example, Khoramishad et al. [20] examined the influence of 3 weight percentages of multi-walled carbon nanotubes on the tensile strength, stiffness, and toughness of the composite laminates. The results showed that the mechanical properties of FMLs were improving with 0.25 and 0.5 wt% of nanotubes, however, with 1 wt% the effect was the opposite - the properties worsened. In another study, where different dosages of nanoclay - from 0.5 to 4 wt% were added to FMLs, samples containing 0.5% had the highest values for toughness and strength [21]. The subject of our study, cellulose nanofibers, has not been studied in detail in the context of fiber metal laminates yet. There is some research regarding the reinforcement of epoxy composites. According to them, cellulose nanofiber-reinforced epoxy composites have excellent thermal and dynamic mechanical properties [6].

Considering the challenges related to nanoparticles and described in the discussed studies is agglomeration. According to Zakaria and Shelesh-nezhad [21], at high concentrations, particles tend to attach to each other and agglomerate which negatively affects the adhesive strength as shown in Figure 1.6.

Therefore, based on the provided data it is crucial to address the problems related to the concentration of nanoparticles and their agglomeration during the experimental part.

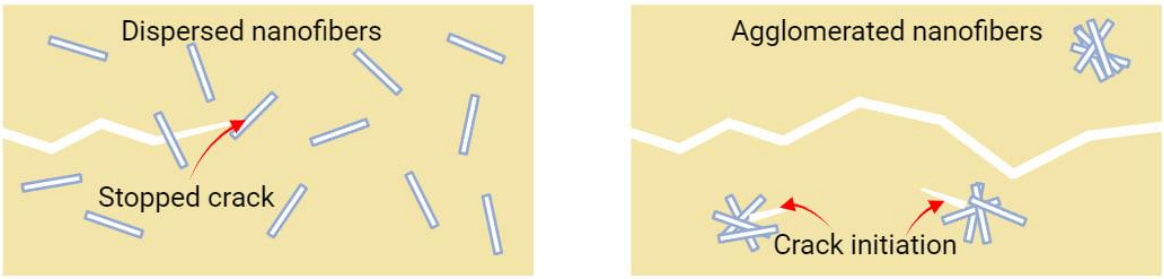

Figure 1.6. Crack propagation in polymer with dispersed and agglomerated nanofibers.

Moreover, another factor considered in the existing research, affecting the strength of the composite material, is the surface roughness of the metal plates. According to Wu et al. [22], the interlaminar shear strength is increased due to the abrasive treatment of surfaces, and it was found that the lower the sandpaper grit, the higher the strength. It can be explained in the way that the size of pores on a rough surface is increased, leading to an increased contact area between the metal, polymer, and nanofibers. According to Mawarni et al. [23], the shear strength of laminate strongly depends on the interlocking mechanism in the interface between the adhesive and the metal. Their research indicates that high surface roughness leads to stronger interaction between the layers of the FML. Purnowidodo et al. [24] investigated that the increase in surface roughness leads to an increase in the tensile strength of FML. There are several approaches to increase the surface roughness of the metal in FMLs. Mehr et al [25] investigated the effect of forest product laboratory etching (FPL), sulfuric acid anodizing (SAA), sandblasting, and combinations of sandblasting with FPL and sandblasting with SAA. The results of this experiment showed that the highest bending strength was achieved for the SAA sample, while the highest strain to failure was reached by the sandblasted sample. In their research Dro´zdziel-Jurkiewicz and Jarosław Bienia´s [26] evaluated the effect of such types of surface treatments as mechanical: sandblasting and

Scotch-Brite abrasion; chemical: P2 etching and phosphate-fluoride process; electrochemical: chromic and sulphuric acid anodizing; plasma treatment and application of sol-gel coatings. The surface analysis has shown that the mechanical methods of surface treatment, especially sandblasting, provide the highest roughness, which ranges from 0.78 to 1.18 μm and changes surface topography, therefore, increasing the surface area. Despite the fact that these methods cannot always provide the desired form of irregularities that ensure mechanical interlocking and adhesive bonding, effective wettability can result in strong and tangible adhesion. Since mechanical surface treatment has proven to be one of the most effective methods and is also more available and affordable than other techniques, it will be used in our research to study the effect of roughness on the adhesive strength between polymer and metal. Due to the limitations of our research, the varying parameter in the mechanical treatment will be the time during which the sandpaper will be applied to obtain a macro-roughened surface and changed topology [3]. The other method of roughening the surface is chemical treatment, which is a simple technique to enhance the single-lap joint bonding. Aluminum is a metal that is a good subtract, which actively forms chemical bonds and reacts to them [27]. According to the study of Zain et al. [28] single lap joints using polyurethane samples were treated with sodium hydroxide and nitric acid, which proved that chemical treatment enhanced overall roughness, surface cleanliness, adhesive bonding, and shear adhesion strength. Both solutions enhance overall roughness, however they have different approaches regarding the reaction with aluminum surface, as NaOH reacts faster and removes the oxide layer. However, HNO_3 removes particles on the surface and further results in corrosion, which again forms a new oxide layer and leads to a rough surface [27].

In order to be able to analyze the effects of roughness on the adhesive strength in FMLs, this property has to be measured and quantified. The core parameters used to describe surface roughness are average roughness *Ra*, root-mean-square roughness *Rq*, and maximum peak-to-valley height *Rt* as presented in Figure 1.7. The first parameter represents the arithmetic average of the absolute values of the roughness profile deviations from the mean line, the second - the root mean square of the roughness profile deviations within the evaluation length, and the third parameter describes the maximum height difference between the highest peak and the deepest valley [29].

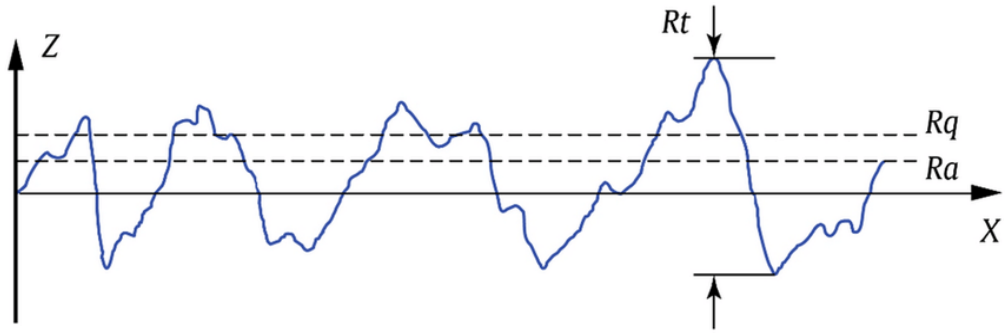

Figure 1.7. Surface roughness parameters Ra, Rq, and Rt [30].

The methods providing information about surface profiles include mechanical, optical, and laser profilometry. Mechanical stylus profilometry involves the contact between a sharp-tipped stylus and a sample surface, enabling the measurement of micro- and nanoscale surface profiles. The technique provides high-precision data on surface characteristics, making it valuable for applications in manufacturing, materials science, and engineering [31]. The optical and laser methods are both non-contact. Optical profilometry utilizes light to measure surface profiles. A structured light source or interference patterns are projected onto the sample surface, and the reflected or diffracted light is analyzed to construct a detailed surface. This method is suitable for delicate or soft surfaces and provides high-resolution measurements [32]. In the laser method, the laser beam is projected at the surface, and the reflection or scattering of the light is analyzed to create a detailed picture of the surface's topography [33]. For our research, the mechanical method is suitable because it is more affordable and is able to provide accurate data for the analysis.

Another parameter that defines how well the adhesive penetrates the asperities and sticks to the metal surface is the contact angle (CA). The property that can be described by this parameter is wettability - the tendency for a liquid to spread on a solid surface. In the research of Wu et al. [34], it was found that a lower water contact angle provides better wettability, therefore increasing the bonding strength between the layers in FMLs. As it is demonstrated in Figure 1.8, the contact angle on a rough surface is less than on a flat one, which means that the droplet sticks to the surface better. According to Guo et al. [35], the wettability can be improved by the addition of surface roughness, however, it is also related to the surface topology. Therefore, some methods of roughening provide better results than others, which should be taken into consideration when assessing the effectiveness of different techniques.

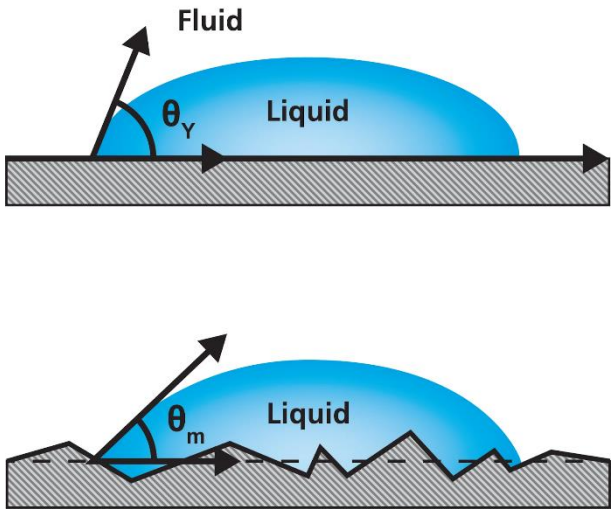

Figure 1.8. Contact angle at the flat and rough surfaces [36].

To do the analytical part of the research, some additional data from mechanical tests are required. Peel and shear pressures are the main factors that affect an adhesive-based junction, however according to Faneco et al. [27], elastic modulus, G values, shear, and tensile strength are not enough to predict joint behavior. Modeling approaches such as cohesive zone modeling (CZM) in actuality rely on both G_{ic}, G_{iic}, and tensile strength of the pure adhesive. When predicting joint strength one of the most important parameters is the G values [37]. Fracture modes such as opening mode (mode 1) and plane shear mode (mode 2) need to go through evaluation of an adhesive necessitates the measurement of several characteristics, including elasticity, ductility, and fracture, each of which calls for specific testing. The most appropriate and easy tests to get G values are double cantilever beam (DCB) and end-notched flexure (ENF) tests. Double cantilever beam (DCB) and tapered double cantilever beam (TDCB) tests are widely used experiments to evaluate the opening mode plane strain energy release rate. After a comparison of both tests, Faneco et al. [37] concluded that the TDCB test is not suitable because ductile properties were not captured, and results did not meet certain conditions of accurate data reduction methods. The same conclusion about the preferability of DCB over TDCB was proposed by Teixeira et al. [38], where the main reason is that DCB is applicable for all types of adhesives while TDCB is only effective for brittle adhesives. For in-plane shear mode in most research 4-point bend end-notched flexure (4ENF), end-loaded split (ELS), and end-notched flexure tests (ENF) are commonly used three tests [39]. ENF test is a widely used and simple method for

assessing the shear performance of adhesive joints to get G_{iic} value. However, crack propagation length results taken from ENF were unstable, which makes its use questionable. In order to prove ENF's adequacy analytical simulation by de Moura [40] was performed to face the problems rising from the crack tip zone. Further improvements regarding uncertainties in the ENF test were researched by Silva et al. [41], which resulted in a great agreement between experimental and analytical results via using the inverse method. For the tensile strength identification, we used a Universal Testing machine, which is according to the standards of adhesive test methods, the most accurate and easy one [42].

3. Materials and methods

3.1 Design of experiments

Based on the reviewed literature, methods to achieve the aims of the research were identified. For this research project a quantitative method of data analysis is used. In order to measure the properties of SLJs and the polyurethane samples both with and without CNF and surface treatment, mechanical tests, including single-lap shear and tensile tests were applied following the ASTM standards. For the single-lap shear and the tensile tests, samples with different weight percentages of CNF in the polyurethane were prepared - from 0 to 2% with an increment of 0.5%. Figure 3.1 shows the flowchart of this project work. It consists of three different parts: Initial project aims, where the hypothesis, purpose and expected outcomes of this project work are presented, 1st stage, where work conducted in the first half of academic year is presented and the 2nd stage, where work conducted in the second half of academic year is presented.

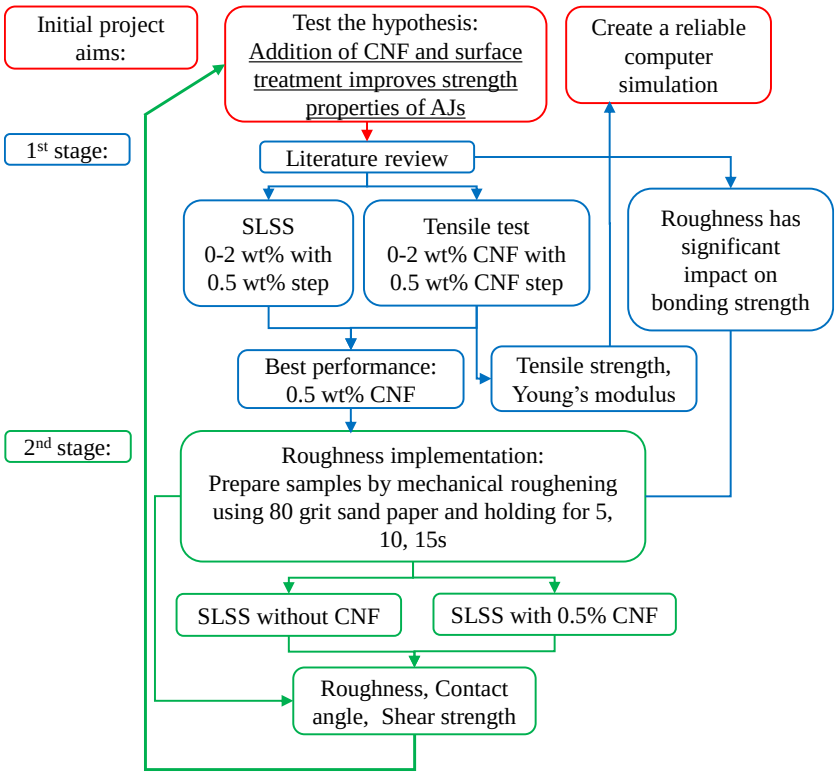

Figure 3.1. Project flowchart.

The first stage consists of literature review which is essential to identify the state of art and find the starting point and targeting areas for the project, initial SLSS and tensile tests to identify the properties of the pure polymer and SLJs without treatment or addition of CNF to obtain reference samples, and testing samples with the addition of different CNF content to investigate its effect and identify the CNF content that results in the best performing samples. The data obtained in this stage is also used to create and verify the computer simulation. The second stage targets the roughness implementation via chemical and mechanical surface treatments, its effect on the strength of SLJs, the synergistic effect of simultaneous surface treatment and addition of CNF on the performance SLJs and identification of the best performing samples. Investigation of nature of the change in strength of the samples is accomplished by the surface analysis of failure surfaces and treated metal surfaces using Surface Electron Microscopy (SEM), Contact Angle measurement (CA) and Roughness measurement. The tentative deadlines for each of the planned tasks are presented as a Gantt chart on Table 3.1

Table 3.1. Gantt Chart.

Task name	September	October	November	December	January	February	March	April
Literature review								
Tensile test of polymer								
SLSS (without CNF)								
SLSS (mechanical roughening)								
SLSS (chemical roughening)								
SLSS (CNF & mech. roughening)								
SLSS (CNF & chem. roughening)								
Data analysis & finishing report								

Taking into account the large number of tests the names of the samples were encoded as shown on Table 3.2 in order to achieve clear presentation of the results. The table consists of different methods used during the experiments. For the experiments targeted to investigate the synergy of different methods both codes were included in the name of the sample. For example, the sample that was mechanically treated for 10 seconds and contained 0.5 wt% content of CNF is named N0.5-M10.

Table 3.2. Codes table.

Code	Description
REF	Reference sample, without the addition of nanofibers and roughness
N0.5	Sample with 0.5 wt% of nanofibers
N1.0	Sample with 1.0 wt% of nanofibers
N1.5	Sample with 1.5 wt% of nanofibers
N2.0	Sample with 2.0 wt% of nanofibers
M5	Samples treated mechanically for 5 seconds
M10	Samples treated mechanically for 10 seconds
M15	Samples treated mechanically for 15 seconds
Ch5	Samples treated chemically for 5 minutes
Ch15	Samples treated chemically for 15 minutes
Ch45	Samples treated chemically for 45 minutes

3.2 Materials and equipment

3.2.1 Materials

1. Aluminum - Al2024 T3 with a thickness of 0.5 mm;
2. Polyurethane - Locally produced by silikon.kz commercial PU-A80 polyurethane;
3. Cellulose nanofibers - Nanografi Cellulose Nanofiber NG01NC0201,

width 10-20 nm, length 2-3 μm, diameter 10-20 nm.

3.2.2 Equipment

1. MTS Criterion C43.304 universal testing machine;
2. HST WDW-3 Electronic Universal Testing Machine;
3. DektakXT Stylus Profiler by Bruker;
4. Scanning Electron Microscope ZEISS Crossbeam 540;
5. BOSCH GSL 180-LI 06019F8109 Screwdriver;

6. Precise electronic weights;
7. Magnetic stirrer;
8. Dataphysics Contact Angle System OCA 45.

3.3 Tensile strength test of polymer

In order to assess the properties of the polymer without metal, and get its tensile strength and Young's modulus for modeling, specimens of polyurethane with different CNF weight percentages were prepared and tested using the tensile test. Firstly, pure polymer with 0 wt% nanoparticles was prepared. Components A and B were taken in a 1:1 ratio by mass, and mixed using a magnetic stirrer for 3 minutes. In cases when the nanoparticles were added, the procedure was changed. First of all, component A was taken and mixed with the measured quantity of CNF for 20 minutes on the magnetic stirrer to avoid the agglomeration of particles. After that, component B of the same mass as component A, was added to the mixture and stirred for 3 more minutes. When the polymer was prepared, it was poured into two metal molds with a length of 28.5 cm and a width of 2.5 cm as shown in Figure 3.2 (a). To get samples of approximately 2 mm thickness, 14 grams of polyurethane was used for each mold. After drying for 1 week, sheets of polymer were taken off the mold and cut into 2 pieces, each 7 cm in length and 2.5 cm in width. The procedure was repeated for all CNF percentages. The final samples before and after testing are presented in Figure 3.2 (b).

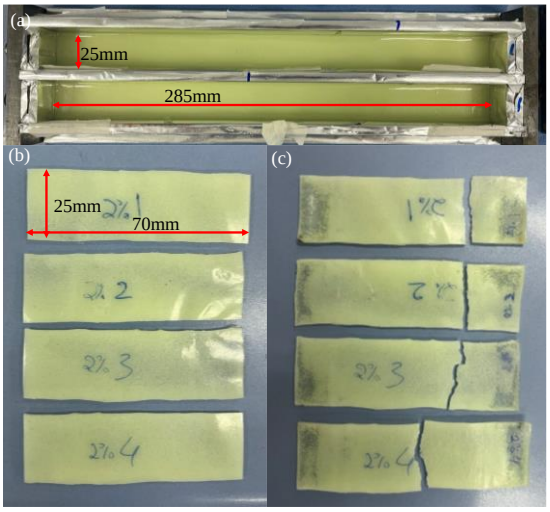

Figure 3.2. (a) Polymer preparation mold with dimensions, (b) PU sample with dimensions, (c) PU sample after testing.

Figure 3.3 shows a schematic of the whole preparation process.

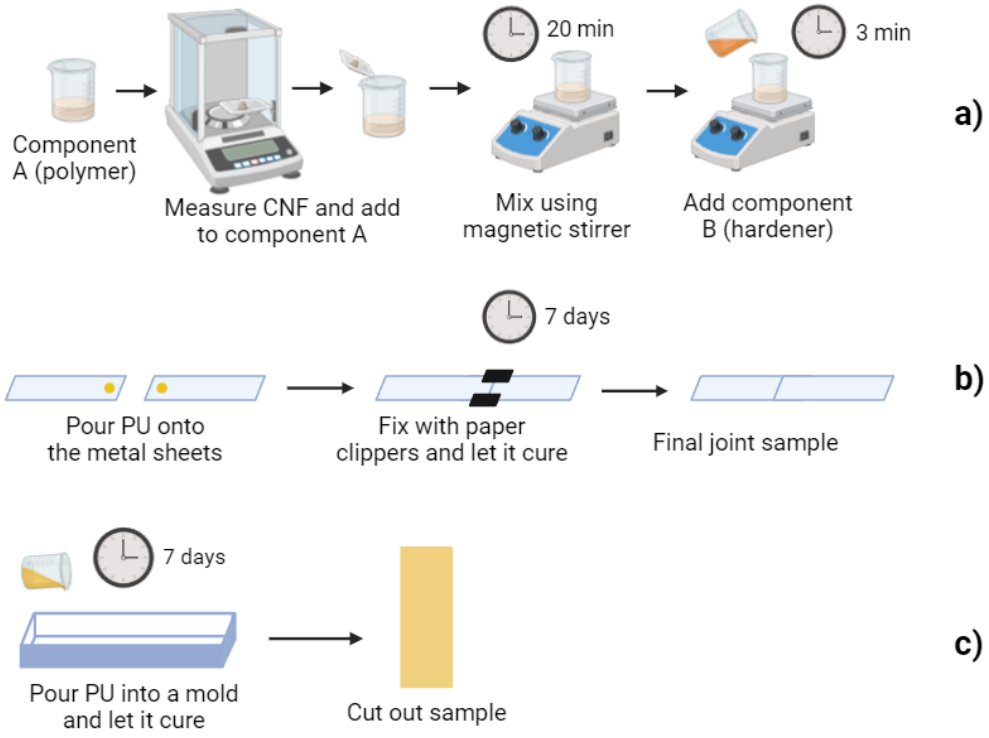

Figure 3.3. (a) preparation of polyurethane with nanofibers; (b) preparation of adhesive joints; (c) preparation of PU samples for tensile test.

The test was conducted on an HST WDW-3 Electronic Universal Testing Machine. A sample of polyurethane was clamped at 2 ends and pulled to the opposite sides at a rate of 10 mm/min. The procedure was repeated for all specimens. A schematic of the machine is shown in Figure 3.4 (a).

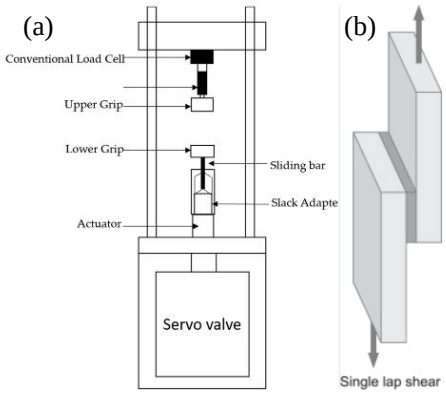

Figure 3.4 (a) Universal testing machine for tensile test, (b) mechanism of single-lap shear test.

3.4 Single lap shear strength test

In order to compare the effect of CNF on the strength of the FMLs, firstly, the pure polymer with 0% nanoparticles was used as the adhesive, and then 0.5 wt% of CNF was added every time till the weight percentage of 2%. The procedure of polyurethane preparation was the same as in the tensile test, described in Section 3.3.1.

The dimensions were taken according to the ASTM D1002 standard. 8 aluminum plates were taken and treated with alcohol to degrease the surface. The needed area for the adhesive presented in Table 3.3 was measured on the metal sheets in order to have the same parameters for all samples, therefore, providing more accurate results. When the polyurethane was ready, it was uniformly distributed on every plate using a medical syringe - the droplets were approximately 0.25 ml. Next, the aluminum sheets were glued together, secured with clips, and left for a week to cure at room temperature. The procedure was repeated for every weight percentage of the nanoparticles in the polymer - 0%, 0.5%, 1%, 1.5%, and 2%.

Table 3.3. Dimensions of single-lap joints.

Parameter	Value
Length of a metal sheet	100 mm
Width of a metal sheet	25 mm
Length of the adhesive	12.5 mm
Width of the adhesive	25 mm
Thickness of the adhesive	0.1 mm
Area of the adhesive	312.5 mm^2

For the single-lap shear test, the MTS Criterion C43.304 universal testing machine was used. Prepared FML samples were fixed with clamps of the machine from 2 ends with contact areas equal to the area of the adhesive. The machine pulled the samples to the opposite sides at the rate of 1 mm/min, giving the load versus crosshead relation in the result. The principle of the test is presented in Figure 3.4 (b).

3.5 Roughness

3.5.1 Mechanical Treatment

Different surface roughness was achieved by treating the metal with sandpaper of grit 80 for three different periods of time: 5 s, 10 s, and 15 s to investigate the effect of different surface roughness on the performance of adhesive joints. For this purpose, a screwdriver with a disc attachment was used as demonstrated in Figure 3.5. A screwdriver with sandpaper glued to the disc was fixed on the platform which can only move in one direction. The platform was equipped with stoppers that stopped it at a fixed distance from the wall where the sample frame was located. The sample was placed inside the frame of the same thickness in order to prevent the thinning of the sheet as it may affect the strength of the adhesive joint. Once all components were fixed, the platform moved to the wall allowing the polishing disc to reach the sample and the screwdriver was turned on for the fixed time. In order to keep the procedure consistent all samples were prepared on the same day, batteries of screwdriver were replaced after every set of 8 samples, and the sanding paper was replaced after every 2 samples.

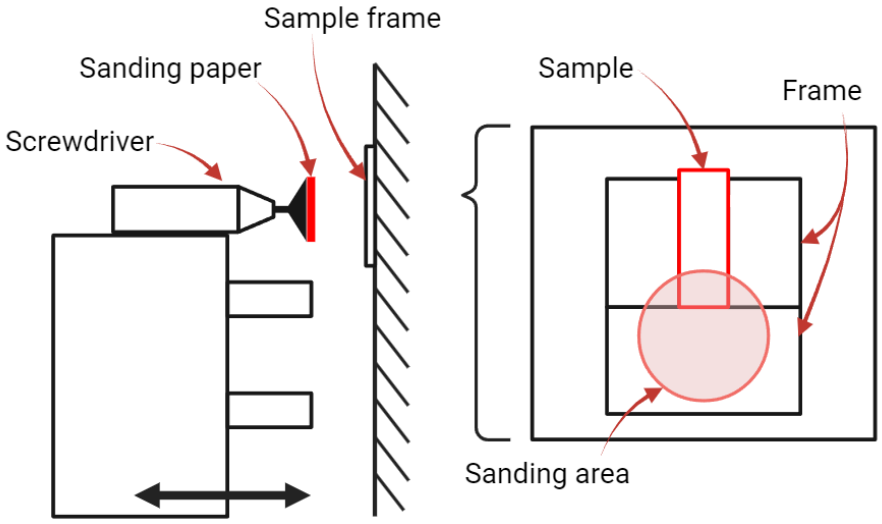

Figure 3.5. Mechanical treatment scheme.

3.5.2 Chemical treatment

The chemical treatment was implemented using a 0.1 M NaOH solution. It was prepared by dissolving 3.2 g of NaOH pills in 800 ml of distilled water by stirring in a circular motion. After preparation, the solution was poured into 40 ml beakers. 2 degreased aluminum sheets were placed in each beaker and left for 5, 15, and 45 minutes, as shown in Figure 3.6. The next step was to place treated sheets into the ultrasonic bath for 5 minutes to remove excess chemicals. Finally, samples were sent to the oven overnight to dry. The final metal sheets were wiped with ethanol.

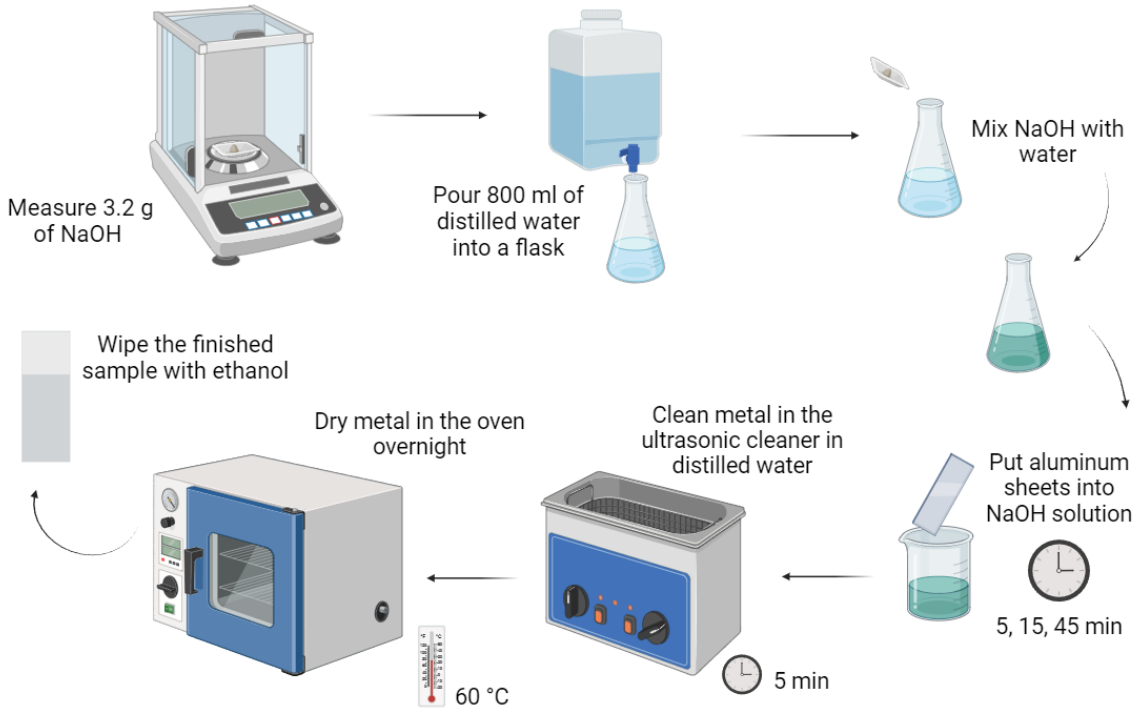

Figure 3.6. Chemical treatment scheme.

3.5.3 Roughness and contact angle measurement

To measure the roughness of aluminum sheets the DektakXT Stylus Profiler by Bruker is used. Since the operating dimensions of the machine is not designed for large samples, small 25x25 mm aluminum sheets, as shown on Figure 3.6 (b), were prepared. Then, these sheets were mechanically and chemically treated, as described in section 3.5.1. and 3.5.2.

For the contact angle measurement, the Dataphysics Contact Angle System OCA 45, presented on figure 3.7 (a) was used. Also, small aluminum sheets, as described in Section 3.5.2 were used due to the same reason. The sheets were located on the platform of the machine and a small droplet of water was placed on it. Since the contact angle does not depend on the volume of the droplet, the exact size of droplets was not controlled via tools but they were kept within a region that can be measured by the system. The tested samples are presented on Figure 3.7 (b).

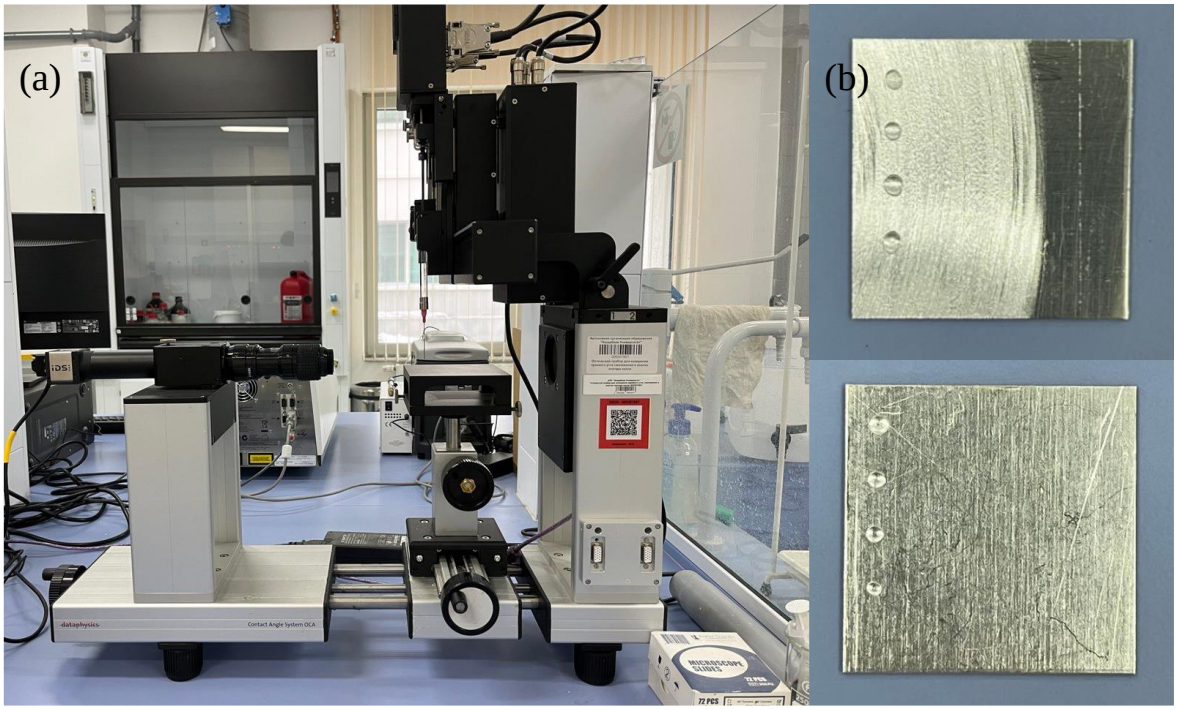

Figure 3.7. (a) Dataphysics Contact Angle System OCA, (b) Contact angle measurement samples after test.

3.6. Modelling

3.6.1 Software

For the modeling part ABAQUS/CAE software was used. The first step is to create the lap shear drawing with the dimensions used in experiments. The thickness of adhesive measured through the experiments is 0.1 mm and the thickness of the aluminum sheet is 0.5 mm. Inside the software, we can create the drawing of SLJ as shown in Figure 3.8.

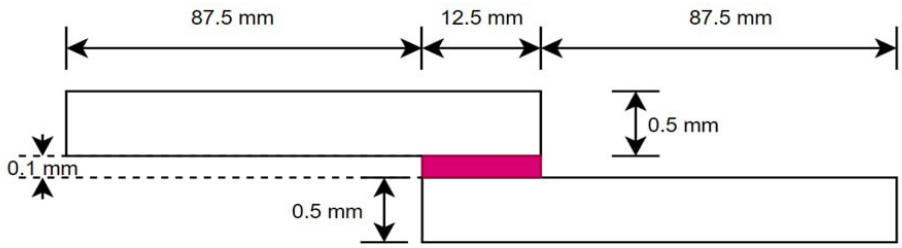

Figure 3.8. SLJ schematic drawing of the part.

Then, material properties were added for adhesive and aluminum sheets as follows as described below.

Aluminum:

- Elastic modulus - 71400MPa
- Poisson's ratio – 0.33

Polyurethane:

- Quads damage - results from the tensile test of the polyurethane were assigned [43].
- Elastic properties - Tensile test stress-strain curve was used to extract values for triangular traction separation law. Stress-strain curve evaluated into stress-displacement curve. Upper boundary green line shows the highest point line, the right boundary red line shows the point before the crack, and the left boundary yellow line represents the elastic zone before the plastic zone. Values taken from the graph are evaluated into the elastic properties [44].

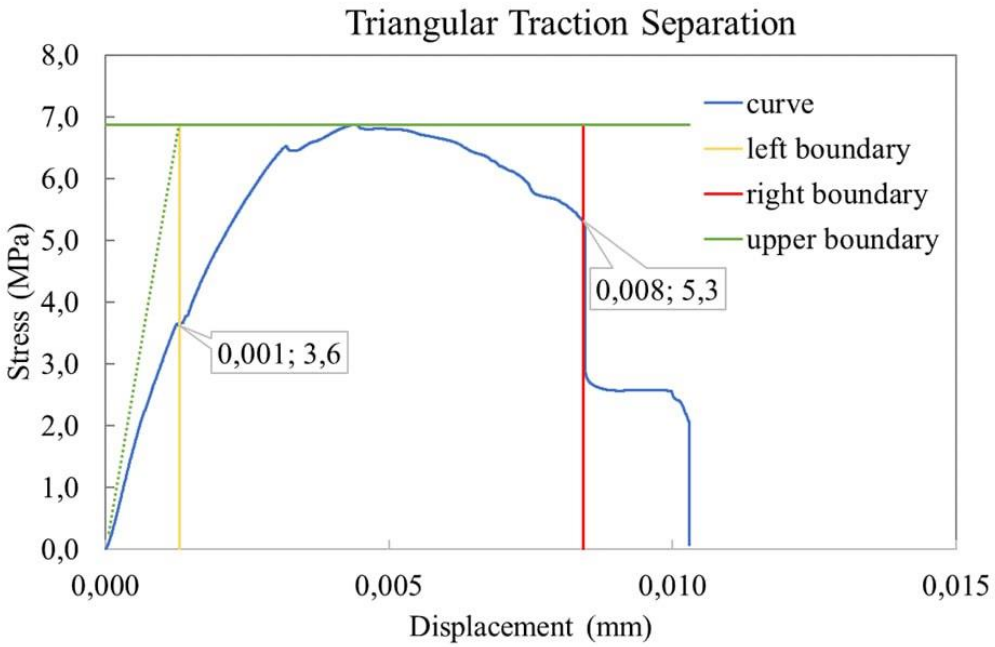

Figure 3.9. Triangular traction separation graph.

- Damage evaluation: For this stage for a pure polyurethane G_{ic} and G_{iic} values are taken from experiments taken from articles. In order to get the appropriate values, we need to compare material properties, especially elastic modulus and tensile strength value. In adhesive properties there are huge differences. As we can see from Table 3.4. elastic modulus of one component polyurethane by Boutar et al. [45] is 2.15 MPa which is lower than our polyurethane component, therefore close one to the expected values is SikaForce TM6 7752-L60 adhesive by Faneco et al. [37]. Values taken from the DCB experiment were 2.313 N/mm as an average value of G_{ic} from three different methods and from ENF test 5.41 N/mm as a G_{iic} value [37].

Table 3.4. Comparison of material properties of adhesive

Parameter	PU-A80 polyurethane	SikaForce TM6 7752-L60 [37].	One component polyurethane [45]
G_{ic}, N/mm	-	2.313	5.905
G_{iic}, N/mm	-	5.41	20.15
Tensile strength, MPa	5.79	11.49	5.4
Tensile strain, %	-	19.18	230
Elastic modulus E, MPa	288.9	493	2.15

The drawing was divided into sections and those sections were assigned to the material with the plane stress/strain thickness of 25 mm and the whole part was assembled into one instance. Boundary conditions were added: one side was fixed and from the other side displacement was added. Incrementation of steps were set as shown in Figure 3.10.

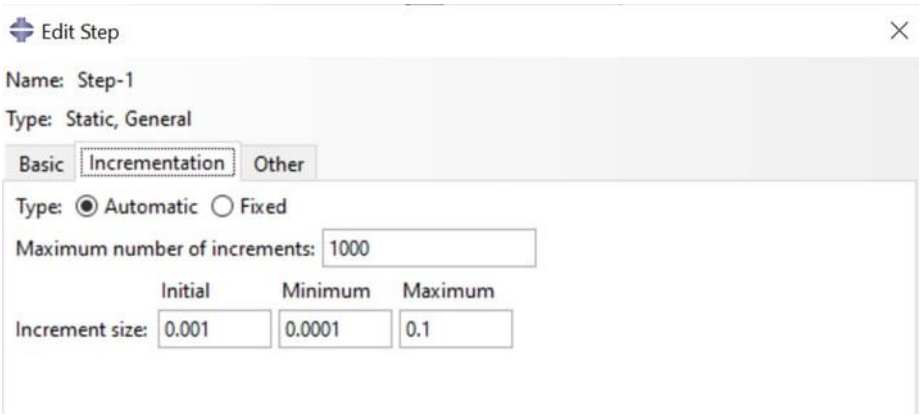

Figure 3.10. Incrementation of steps

The last setup is meshing, mesh size for this model is 0.09, through mesh sensitivity analysis appropriate mesh size was determined and the best results were achieved. Finally, after all setups were done a job was added and ran.

4. Results and Discussion

4.1 Tensile test

4.1.1 Tensile strength

From the tensile test results, it can be seen that the addition of CNF significantly improved the tensile strength of polyurethane with 0.5 and 1 wt% of the nanomaterial. In comparison to the reference sample, the tensile strength of polyurethane with 0.5 wt% has increased by 308% times, while with 1 wt% - by 401%. It can be explained by the fact that cellulose nanofibers have a high aspect ratio (length divided by diameter), therefore, enhancing mechanical properties such as flexural strength and modulus, and tensile strength due to increased entanglement and effective reinforcement within the polymer [74]. Starting from 1.5 wt% CNF, there is a sharp decrease in the tensile strength. This trend is observed with many types of nanoparticles and is most probably related to their property to agglomerate. The agglomerated clusters can act as stress-concentration sites during tension, thus leading to the reduced aspect ratio of CNF, and consequently, to the reduction of mechanical properties including tensile strength and Young's Modulus [75]. A similar behavior of CNF was observed in the combination with epoxy. In their research, Saba et al. [46] studied the effect of different wt% of nanofibers, 0.5, 0.75, and 1, on the mechanical properties of reinforced epoxy composites. 0.75 wt% of nanofibers gave a 25% increase in the tensile strength, and 1 wt% led to its decrease. Even though their percentage increase was not as high as in our results, which may be related to the difference in the used polymers, it can be concluded that when the concentration of the CNF becomes too big, the effect of their clustering becomes significant.

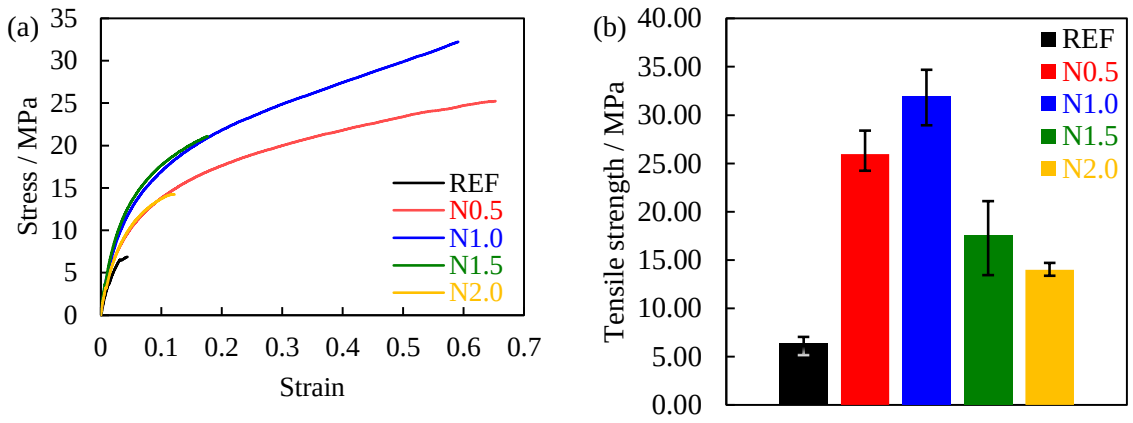

Figure 4.1. (a) Stress-strain curves of samples with 0 (REF), 0.5 (N0.5), 1.0 (N1.0), 1.5 (N1.5) and 2 (N2.0) wt% CNF and (b) Tensile strength of samples with 0 (REF), 0.5 (N0.5), 1.0 (N1.0), 1.5 (N1.5) and 2 (N2.0) wt% CNF

4.1.2 Young's modulus

Referring to Young's modulus values, they show a similar trend as tensile strength. As shown in Figure 4.2, there is a gradual growth of the average Young's modulus with the increase of CNF concentration up to a point of 1 wt% CNF, when E = 481.31MPa, giving a 66.6% increase, followed by a steady decrease of Young's modulus with further addition of CNF. However, compared to the tensile strength, the decrease of Young's modulus was not as big after 1.5 wt%. As Young's modulus is a parameter that measures the elasticity, the ratio of the stress to the strain produced, it can be seen how nanofibers reinforce the polymer by distributing the stress throughout the material, limiting crack propagation, and increasing the resistance of polyurethane to deformation. The large aspect ratio of CNFs and their entanglements, assisting in fiber-matrix and fiber–fiber load transfers, facilitates the early occurrence of the strain hardening of the composite material [81]. In another research, which was conducted using starch biopolymer, the addition of 0.5 wt% CNF provided a 170% increase in Young's modulus, after which there was deterioration [82]. The difference in the percentage increase may be due to the difference in the materials, because polyurethane initially had quite a high Young's modulus, however, the mechanical behavior in both cases is similar, which supports our obtained results.

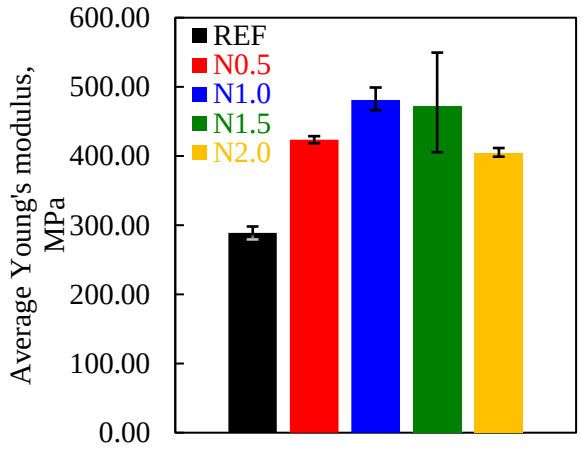

Figure 4.2. Young's modulus of samples with 0 (REF), 0.5 (N0.5), 1.0 (N1.0), 1.5 (N1.5) and 2 (N2.0) wt% CNF

4.2 Effect of nanofibers on shear strength

The results of the lap shear tests conducted for different concentrations of cellulose nanofibers (CNF) are presented in this section. The concentrations of nanofibers in the samples were 0.0 wt%, 0.5 wt%, 1.0 wt%, 1.5 wt% and 2.0 wt% based on the findings of other research works. From the conducted experiments it was confirmed that the addition of CNF has significant impact of the shear strength of SLJs and the content of CNF in the polymer plays a major role in the overall performance of SLJs. From the experimental results presented on Figure 4.3, it can be seen that the reference sample with 0 wt% of CNF has the lowest shear strength, as it only achieved 1.09 MPa, and the smallest displacement of 0.2 mm. The addition of 0.5 wt% CNF has significantly enhanced both parameters. The shear strength increased by 86% in comparison to the reference sample, amounting to 2.03 MPa, while the displacement increased tenfold reaching 2.1 mm. However, it can also be observed that the addition of higher content of CNF from 1 wt% to 2 wt% decreased the strength of the adhesive joints. N1.0 and N1.5 samples only reached strength of 1.6 MPa, while N2.0 sample's strength dropped almost to the level of the reference sample and reached 1.1 MPa.

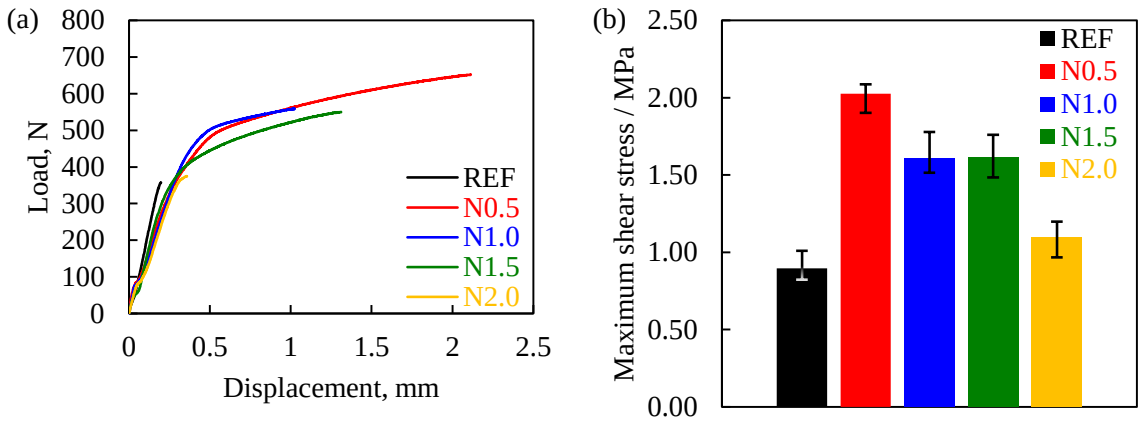

Figure 4.3. SLSS tests (a) typical load-displacement curves of samples with 0 (REF), 0.5 (N0.5), 1.0 (N1.0), 1.5 (N1.5) and 2 (N2.0) wt% CNF, (b) maximum shear stress values of samples with 0 (REF), 0.5 (N0.5), 1.0 (N1.0), 1.5 (N1.5) and 2 (N2.0) wt% CNF

As expected, the achieved results correlate with the SLSS test results achieved in studies of different nanocomposites. In their study on shear and flexural strength of single lap composite joints with graphene nanoparticles (GNPs) Venugopal and Sudhagar observed that GNPs increased the shear strength of joints by 69.4% at 0.75 wt% content and it steadily decreased with the further increase of GNPs' content [76]. Charitidis, investigating Al-Epoxy SLJs with the addition of Alumina nanoparticles, also observed the peak of strength at 0.5 wt% nanoparticle content with the following decrease in strength at higher content [77]. The results of these SLSS tests supports the claims made in earlier chapters. As it was discussed in Chapter 2, the improvement of strength properties with the addition of CNFs is related to their large aspect ratio and mechanisms, preventing crack propagation, such as nanofiber bridging, crack deflection and crack arrest associated with it [18], while the decrease in strength is related to the fact that at high content nanofibers tend to agglomerate creating clusters in the adhesive and losing their high aspect ratio. These agglomerations in the form of craters in the polymer and on the metal-adhesive interface become stress concentrators and, therefore, act as crack sources if stress concentration is beyond critical local strength reducing the bonding strength [78]. Moreover, based on the study of nanoclay particles, it was found that their agglomeration prevents the infiltration of an adhesive into porous structures of the aluminum layer and consequently, reduces the interlaminar shear strength [79].

4.3 Effect of surface treatment

4.3.1 Mechanical treatment

Figure 4.4 represents the results of the single-lap shear test for joints with mechanical surface treatment. In comparison to the reference sample, which was not exposed to any treatment, specimens with roughness obtained by mechanical means show a substantial increase in both - displacement and shear strength. The highest values were obtained by treating aluminum sheets for 10 seconds with sandpaper - the shear strength reached 2.08 MPa giving 90.8% increase, while displacement reached 3 mm. Samples treated for 15 seconds have slightly lower strength, 1.98 MPa, but displacement is 2 times smaller, accounting for 1.5 mm.

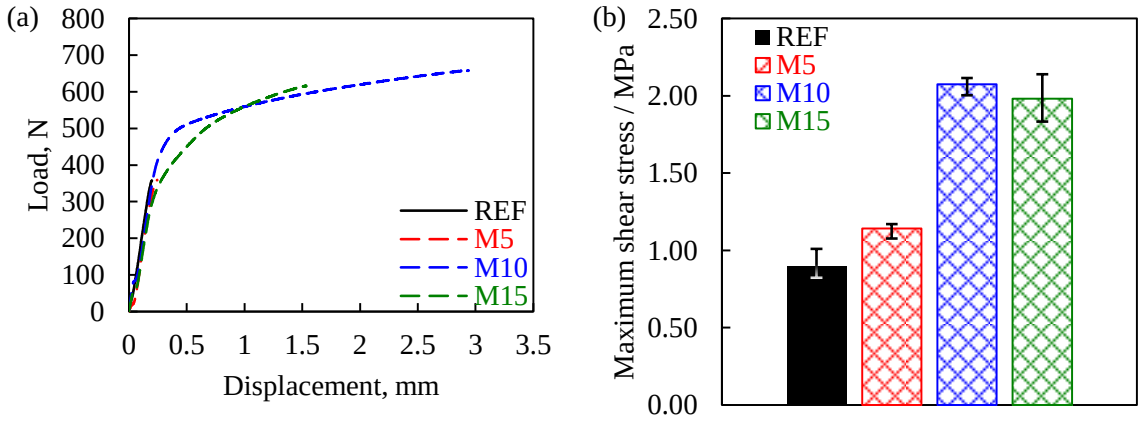

Figure 4.4. a) Typical Load-displacement curves obtained from single-lap shear tests of 5 (M5), 10 (M10) and 15 (M15) s mechanical treatment, (b) Shear strength obtained from single-lap shear tests of 5 (M5), 10 (M10) and 15 (M15) s mechanical treatment.

One of the reasons leading to increase of shear strength of SLJs is associated with a better wettability of treated surfaces. As shown on Figure 4.5, CA values for M5, M10 and M15 samples decreased by 27.23, 19.43 and 26.35° respectively. Sample treated for 5 s had strength of only 1.14, which is only a 4.6% increase. In the case of the 5-second treatment, there was only a minor increase in strength and almost no difference in displacement, compared to the reference sample. It may be explained by the fact that the time was not enough to cover the whole surface uniformly, leaving the surface with sharp peaks.

Therefore, a large number of stress concentration points were introduced leading to crack initiation and its fast propagation.

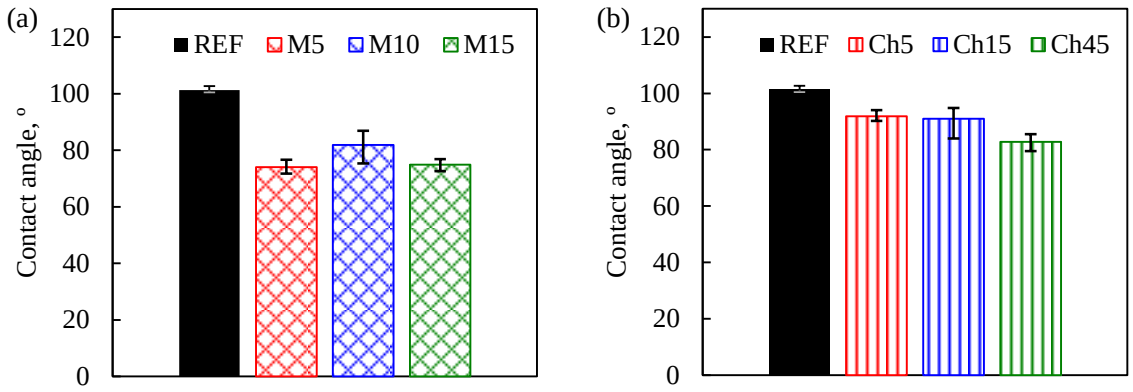

Figure 4.5. Contact angle of (a) mechanically and (b) chemically treated samples

This claim can be verified by the roughness measurements of mechanically treated aluminum sheets presented on Figure 4.6(b, c, d). It is clearly seen that aluminum sheet that was treated mechanically for 5 seconds has significantly larger number of short and thin peaks and valleys, while samples treated for 10 and 15 seconds, due to a longer polishing time obtained wider valleys that can be filled with polymer without leaving any gaps. Another observation from the roughness measurement results presented on Figure 4.6 (a), is that the shear strength of SLJs is not directly related to the average roughness of the surface of the metal. The behavior of SLJs indicate that there is an optimal roughness value that gives the highest strength. The similar behavior was observed by Khan et al. as different SLJs made of aluminum alloys and steel with different epoxy adhesives had certain roughness value giving the highest strength and both decrease or increase of roughness led to the decrease of strength [80]. The optimal roughness value for aluminum SLJs obtained in their research was 0.83 µm, while our test results show that the optimal value was 3.27 µm achieved by 10 s mechanical treatment. The difference in these values is explained by the different materials used to make SLJs, since the optimum surface roughness is dependent on the type of adherend and adhesive materials [80].

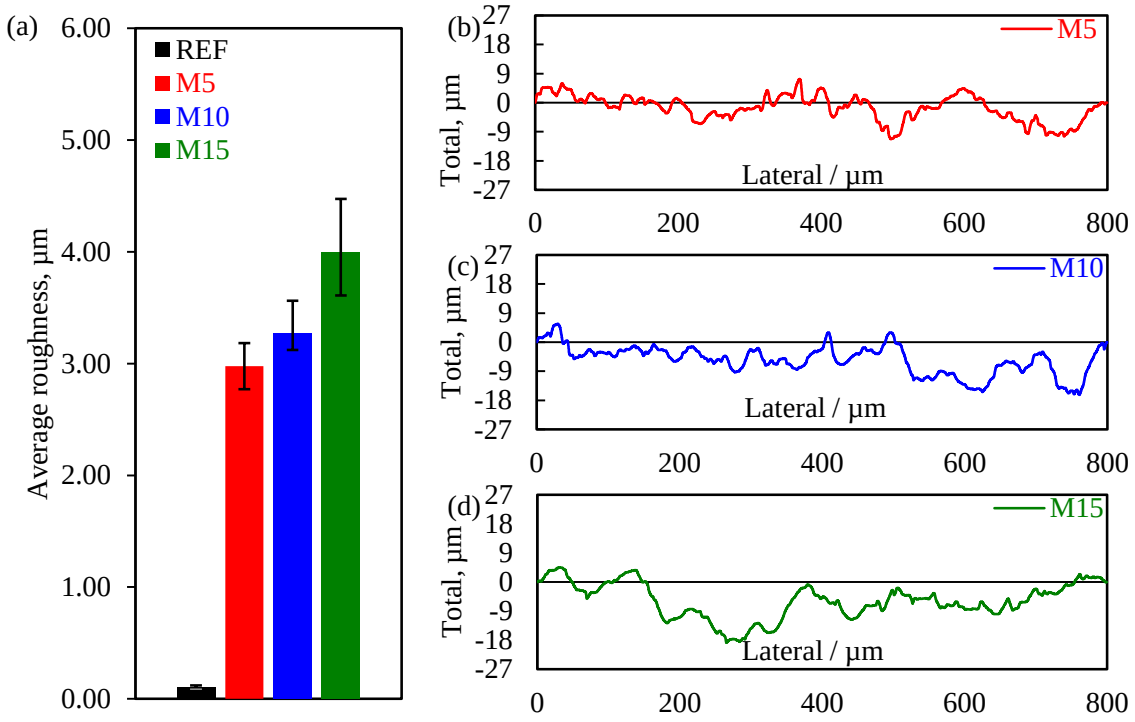

Figure 4.6. a) Average roughness of aluminum sheets treated mechanically for 5 (M5), 10 (M10) and 15 (M15) s compared to untreated sheet and roughness profiles of aluminum sheets treated mechanically for (a) 5 (M5), (b) 10 (M10) and (c) 15 (M15) s

4.3.1 Chemical treatment

Figure 4.7 (b) shows the data obtained for the single-lap shear test for samples with chemical surface treatment using NaOH solution. The highest value was reached by samples that were treated for 45 minutes substantially enhancing shear strength up to 1.93 MPa, which gives a 77% increase in comparison to the untreated reference sample. Moreover, considering Figure 4.7 (a), these samples also provide the biggest displacement of 0.4 mm. Samples treated for 5 and 15 minutes showed a minor improvement in strength. As described in similar research, where the effect of chemical etching's time variation on the shear strength was studied, treatment for a little time only cleans the surface from organic contaminants that were not removed by degreasing, but after sufficient time NaOH etching makes microroughness on the surface [83]. The results for roughness are discussed in more detail in the next section. In general, the reason behind the increased shear strength in the adhesive joints is the

mechanical interlock provided by the enlarged intersection area due to roughness.

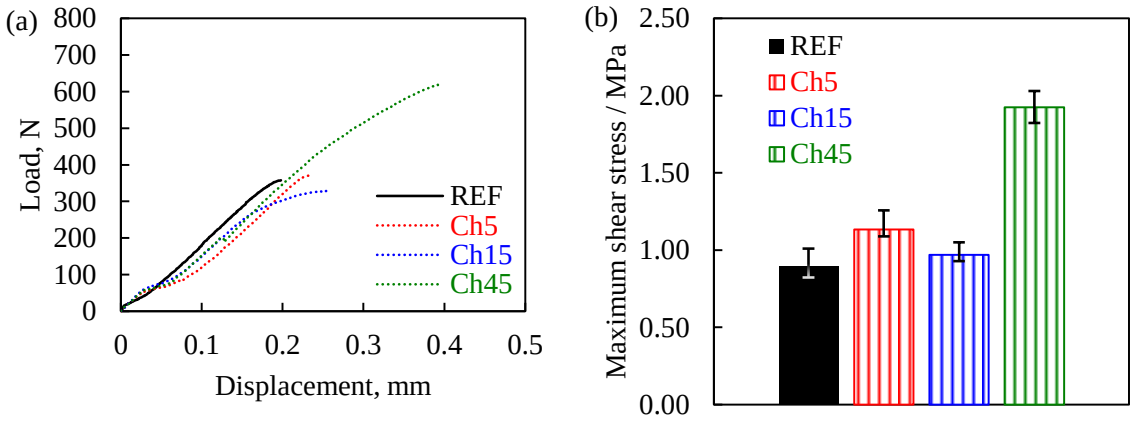

Figure 4.7. a) Typical Load-displacement curves obtained from single-lap shear tests of 5 (Ch5), 15 (Ch15) and 45 (Ch45) m chemical treatment, (b) Shear strength obtained from single-lap shear tests of 5 (Ch5), 15 (Ch15) and 45 (Ch45) m chemical treatment.

In comparison to mechanical treatment, which makes macro roughness on the metal surface, chemical etching gives microroughness. From the bar chart provided in Figure 4.8 (a), the highest average roughness was obtained after 45 minutes of surface treatment accounting for 0.365 m. In the surface profile presented in Figure 4.8 (b, c, d), there is a minor change in the total roughness of specimens treated for 5 and 15 minutes in comparison to the reference sample. If 45 minutes of treatment increased roughness by 246% compared to the untreated surface, 5 and 15 minutes gave the increase of 65.6% and 95% respectively. In addition, chemical etching changes the topography of the metal surface to a pitted one, which is typical for aluminum alloy etched in alkaline solutions. The longest chemical treatment makes micropores on the surface, therefore, allowing the polymer to penetrate into them, providing better interfacial adhesion [84].

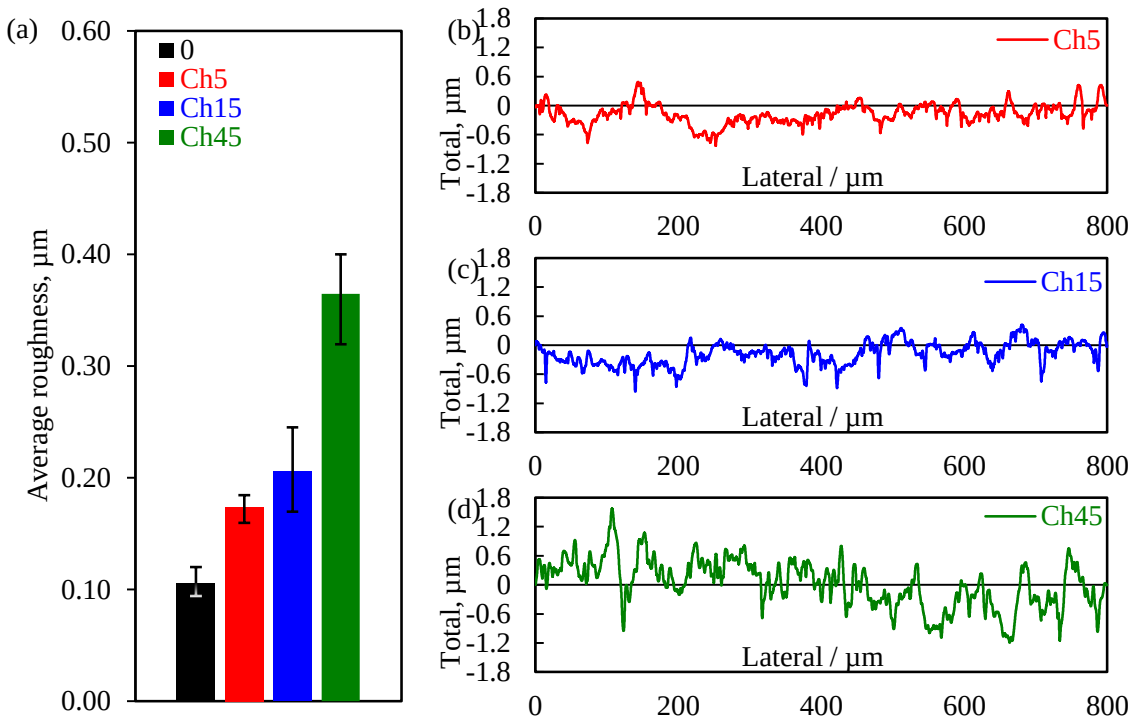

Figure 4.8. a) Average roughness of aluminum sheets treated chemically for 5 (Ch5), 15 (Ch15) and 45 (Ch45) m compared to untreated sheet and roughness profiles of aluminum sheets treated chemically for (a) 5 (Ch5), (b) 15 (Ch15) and (c) 45 (Ch45) m.

4.4 Synergistic effect

The findings of the single-lap shear tests of treated samples and adhesive joints with CNF have shown that both of the methods positively affect the interfacial strength of the adhesive joints. Consequently, their synergistic effect was also studied. As mechanical treatment and chemical etching are both types of surface treatment and add roughness to the metal sheets, they were not combined. Instead, nanofiber-reinforced polyurethane with 0.5 wt% of CNF was used to prepare samples with treated metal sheets. The single-lap shear test results presented in Figure 4.9 (b) and Figure 4.10 (b), show that in the case of the synergy of nanomaterial and mechanical treatment, the best results for the shear strength were obtained with 5 seconds of treatment amounting to 2.53 MPa, while for the chemical etching, the highest value of 2.58 MPa was achieved with treatment for 45 minutes. Mechanical treatment

combined with the usage of CNF increased the shear strength by 132%, and the chemical - by 137% compared to the reference sample.

It can be noticed from the results that mechanical treatment without nanofibers gave the best strength after 10 s, while with CNF - after 5 s. A possible reason for this can be surface morphology after treatment. As shown in Figure 4.11, and discussed in previous sections, mechanical treatment creates macro roughness on the surface. For this reason, there are voids formed where the polymer cannot penetrate [85], which can be observed in the SEM images in Figure 4.11 (f). If we add nanofibers to this kind of structure, it will block the penetration of polyurethane even more, deteriorating the bonding strength.

Considering the chemical treatment, the obtained results can be explained by aluminum surface microstructure and morphology. According to Wu et al. [86], who studied the synergistic effect of surface treatment and graphene oxide interleaf for delamination toughening, alkali etching of aluminum provides plenty of micro holes and valleys, allowing the nanofibers to fill them up and enhance interlock. This can be seen in Figure 4.11, on the SEM images of the tested samples. The size of the holes allows good adhesion of the nanofibers to the surface and additionally increases the contact area.

Discussing the displacement, if for mechanical treatment the biggest displacement is also given by the samples treated for 5 s, samples treated for 5 minutes with chemical etching gave a better result with just a little difference in the shear strength compared to 45 minutes. Therefore, it may be more efficient to use nanofibers and a 5-minute chemical treatment rather than a 45-minute treatment.

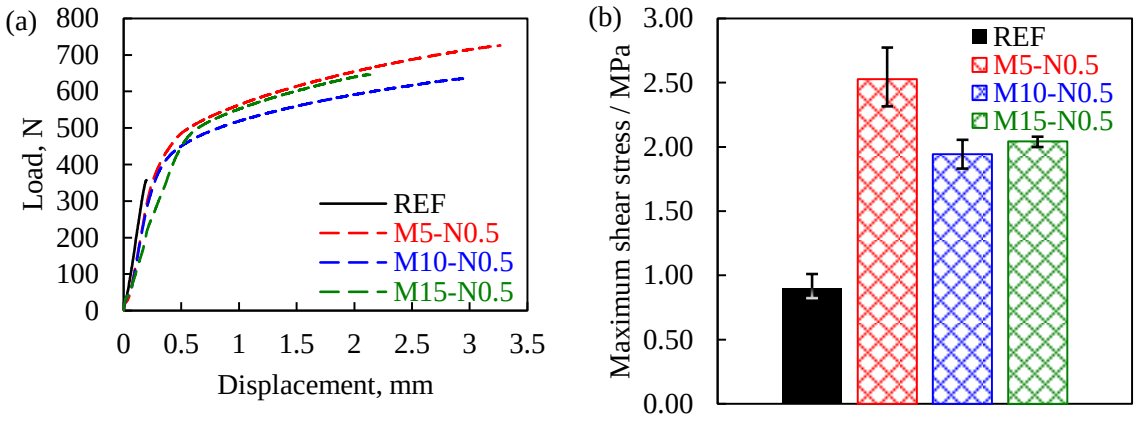

Fig 4.9. (a) Load vs displacement curves of 5, 10, 15 s mechanical treatment with 0.5 wt% CNF, (b) Maximum shear stress of 5, 10, 15 s mechanical treatment with 0.5 wt% CNF.

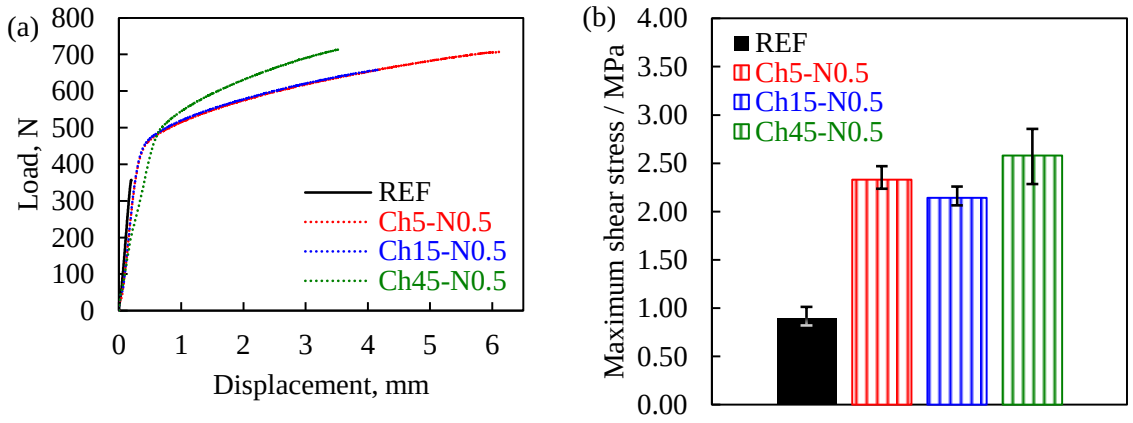

Fig 4.10. (a) Load vs displacement curves of 5, 15, 45 m chemical treatment with 0.5 wt% CNF, (b) Maximum shear stress of 5, 15, 45 m chemical treatment with 0.5 wt% CNF.

4.5 Interface analysis

The different effect of surface treatment methods and CNF addition on strength of joints is related to the type of roughness of the metal and ability of PU to penetrate into the formed pores and activate interlocking mechanism. Figure 4.11 illustrates the PU-Al interfaces without and with different surface treatments. As it can be seen from Figure 4.11 (a), the metal without surface treatment has lowest contact area and no mechanical interlock, while interface of mechanically treated SLJs has deep groves theoretically leading to the best mechanical interlock. However, Figure 4.11 (b) also shows the formation of air gaps in the interface of samples treated mechanically. PU cannot penetrate the grooves due to high viscosity of polymer and narrow and deep valleys resulting in stress concentration points and crack initiation in the gaps. The size of valleys was increased via a longer duration of mechanical abrasion which led to polishing of sharp peaks and elimination of stress concentration points. This resulted in higher strength of M10 and M15 SLJs as shown on Figure 4.4. Contrary to mechanical treatment, chemical treatment results in a less rough

wave-like surface, as shown on Figure 4.11 (c), which to the better distribution of polymer on the surface without forming air gaps.

The expected behavior was observed on the SEM images presented of Figure 4.11 (e-h). The picture of reference sample on Figure 4.11 (e) shows that surface of the metal is smooth, having only rolling lines and the polymer was easily detached from the metal. It indicates that the surface has low wettability and no mechanical interlock leading to the lowest strength of the SLJs.

The example of mechanical interlock in action can be observed on the Figure 4.11 (f) as polymer stretches from the deep groves made by mechanical roughening leading to the increased shear strength of SLJs. This picture also shows the formation of air gaps as it is clearly seen that the grooves are not filled completely and there is a major presence of not filled space on the surface of the metal.

The effect of chemical treatment on the dispersion of PU on the surface of the metal can be seen from the Figure 4.11 (g). The surface of interface differs significantly from the mechanically treated SLJs, as the metal surface has wave-like structure with micro-roughness which allows PU to cover the whole surface. The darker regions, like the one indicated on the Figure 4.11 (g), indicate the area with the residue PU after the major chunk was detached. It is seen that the PU covers all the cavities formed as a result of chemical treatment and no empty voids as observed on Figure 4.11 (f) are present.

Figure 4.11 (h) shows how the CNF strengthen the SLJs via the mechanisms discussed in previous chapters. The effect of high aspect ratio of CNF can be observed on the nanofiber pullouts shown on the region indicated by 1. The nanofibers were pulled out during the breaking meaning that they have strong bond with PU and that CNF bear significant amount of load. The region indicated by 2 shows the example of bridging by CNF. The accumulation of these factors led to the strongest SLJs with to strength improved by 136.7%. The obtained results also verify the claim that the highest strength is achieved when the failure mode is purely cohesive [80]. As it can be seen from Figure 4.11 (i), failure mode of reference sample was purely adhesive, while fracture surfaces of chemically treated samples were semi-cohesive. Figure 4.11(g) shows that the surface contains mostly cohesive failure regions with adhesive failure on the sides. On the other hand, failure surfaces of

mechanically treated samples were purely cohesive, however they contain a large number of cracks which were cause by the large roughness and air gaps, as discussed earlier. Therefore, both of surface treatment methods resulted in a similar increase in strength, 77.1 and 90.8 % for chemical and mechanical treatments respectively. The strongest combination of chemical treatment for 45 minutes and 0.5 wt% CNF content had purely cohesive failure without noticeable cracks.

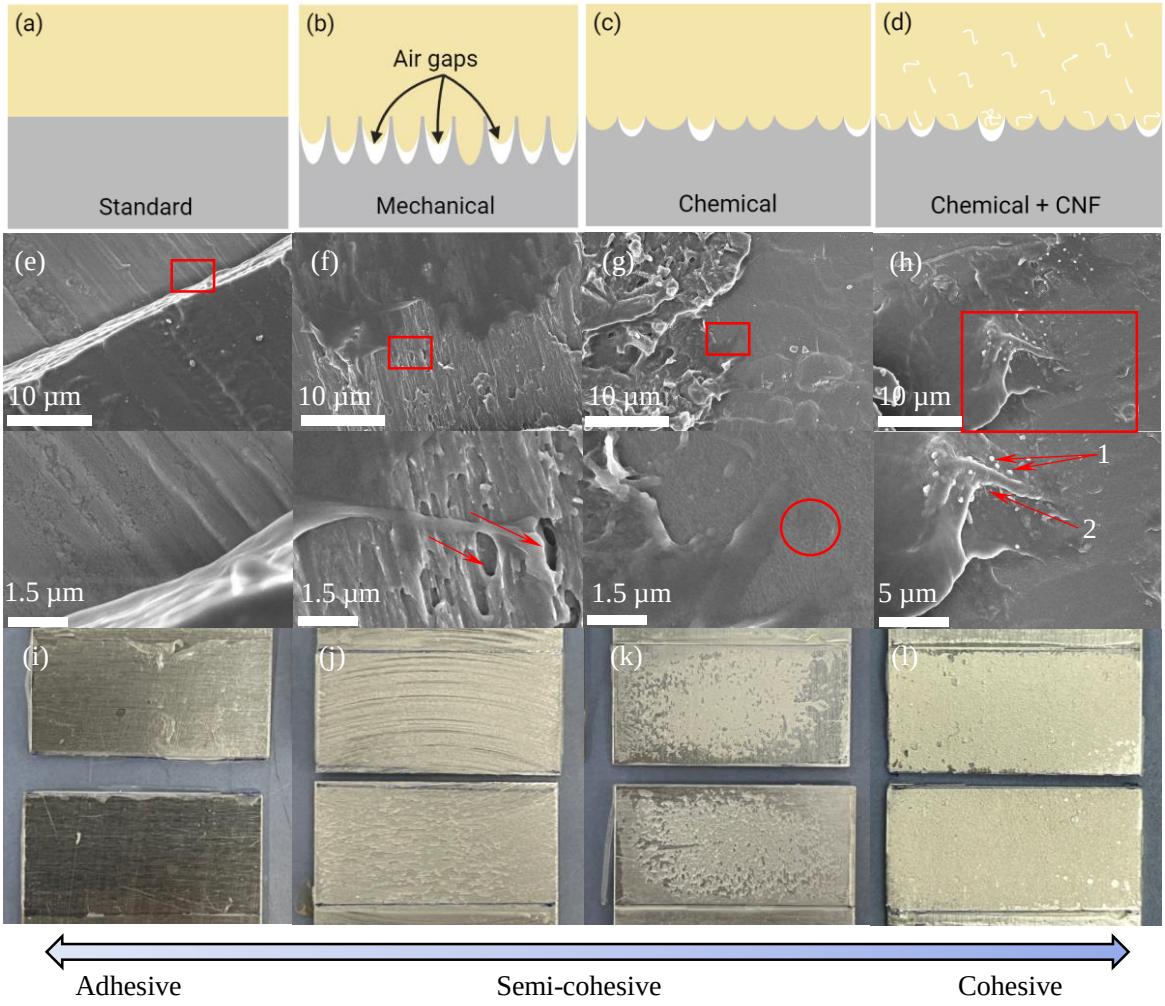

Figure 4.11. Schematic comparison of PU-Al interfaces (a) as received, (b) after mechanical treatment and (c) after chemical treatment (d) chemical treatment + CNF, SEM images of fracture surfaces of (e) REF, (f) M5-N0.5, (g) Ch45 and (h) Ch45-N0.5 samples, pictures of fracture surfaces of (i) REF, (j) M5-N0.5, (k) Ch45 and (l) Ch45-N0.5 samples

4.6 Modeling

Numerical modeling was carried out to show the simulation of mechanical properties of the single lap joint of the actual experiment carried out in the laboratory. The main advantage of using modeling is the structure analysis is easy to perform and with multiple embedded functions of the software. Secondly, fracture damage behavior on the joints can be simulated through cohesive zone modeling (CZM), which helps to accurately predict failure loading, displacement and deformation [87]. In the application of CZM, the most important fracture characteristics needed are the critical strain energy release rate value [88]. Those values are calculated through triangular traction separation method and used in the modeling.

Results section in the software include output field requests that were selected beforehand: how adherent is damaged (SDEG), stress distribution (S), strain (LE) and reaction force (RF). Mesh size for the given model was 0.09 which is the same as the thickness of the adhesive, where 13471 elements have been generated.

Finding a proper mesh size, incrementation and elastic property data is directly related to convergence problem solving. In the visualization side we can see our results. For the evaluation of the simulation to be done correctly, damage evaluation should be close to 0.99 and in load-displacement graph peak points should be reached to be close to experimental values. Figure 4.12 shows that the damage evaluation value is 99%, which shows total damage propagation of the adhesive.

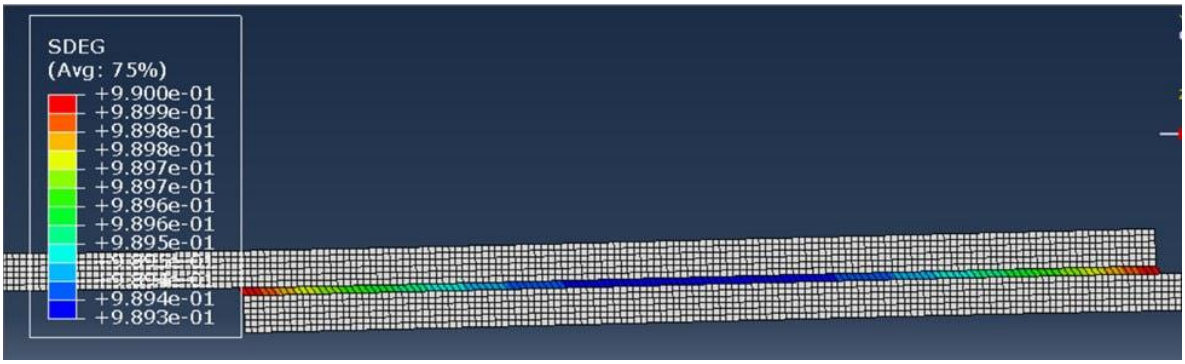

Figure 4.12. Damage propagation

Figure 4.13 shows the maximum load applied for one end of the adherent, which is 469.6 N, while the maximum load value applied in the experimental part was 315.9 N, which

is approximately 1.5 times less than the simulation part results. Such a difference can be explained by the values taken from the papers, as the material properties of the polyurethane were approximately 1.7 times bigger than the experimentally taken value of elastic modulus (E). According to Campilho et al. [87] and Pinto et al. [89], studies carried out both experimentally and numerically show that both are accurately close to each other, however the samples which were experimentally wrong showed different results from the modeling. Therefore, it shows that if G values were taken from the experiments, then the results would be approximately the same.

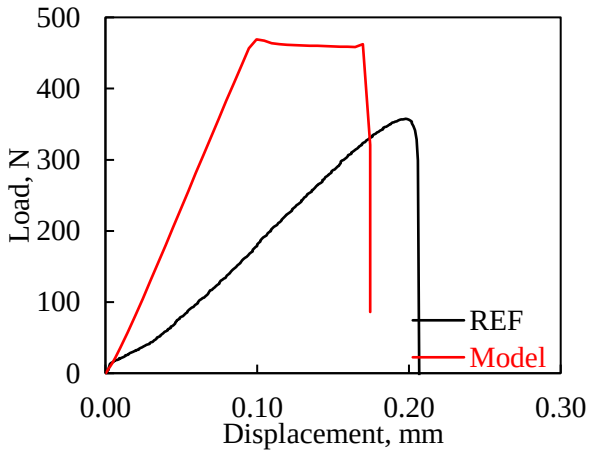

Figure 4.13. Force vs Displacement graph of experimental sample and simulation

Overall, from Figure 4.14 the stress distribution over the part can be seen in gradients. Mostly stress was applied in the inner corners of the single lap joint, where the simulation demonstrates cohesive failure of the adhesive material. The results of the applied force can be seen from Figure 4.14. The left-hand side of the SJL was fixed, while to the right-hand side a concentrated force was applied. It is mainly affecting the left-hand surface, as the other part if fixed with no force affecting. According to the results of pure polyurethane simulation, displacement values showed approximately similar results to the experimental values, however maximum load values were different due to input values were taken from the literature. However, as the material properties of the adhesive taken from papers and the PU used in this project differ from each other, which affects the results of modeling compared with experimental results. Following outcomes proved that similar simulations could be performed for an adhesive with the addition of nanoparticles. Furthermore, in order to get proper results DCB and ENF should be done experimentally and G values for different

weight percentages of nanoparticles should be evaluated. In order to do simulation for different weight percentages of nanoparticles we needed G values. Unfortunately, there was not enough data in the papers for polyurethane with CNF content of 0.5-2 wt%.

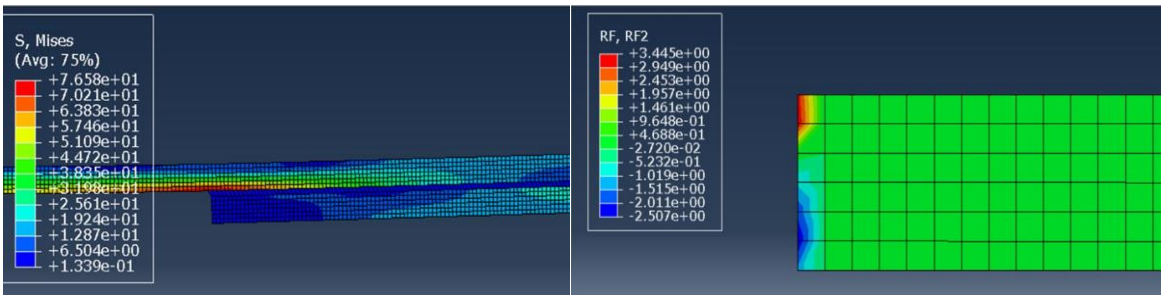

Figure 4.14. Stress distribution (S) and Reference Force (RF).

5. Conclusion and Future work

In conclusion, the research was done to study the interfacial strength in the layers of composite to identify how the addition of nanoparticles, surface treatment methods, and their synergy in adhesive joints would affect the mechanical properties. The study was implemented using both - experimental and numerical methods. The following outcomes can be concluded according to our research experiments and simulation:

- The tensile strength and Young's modulus of the polyurethane were studied: the results showed that 1 wt% gave the highest values due to the high aspect ratio of CNF. 1 wt% of CNF increased tensile strength by 401% and Young's modulus by 66.6%. These values were successfully incorporated into the simulation;
- Single-lap shear strength of polyurethane aluminum joints with cellulose nanofibers: with the addition of 0.5 wt% of CNF, the shear strength has increased by 86% in comparison to the reference sample. However, 1 wt% to 2 wt% of CNF decreased the strength of the adhesive joints due to their agglomeration. The simulation of the single-lap shear test for 0 wt% has a moderate accuracy and closely resembles the experimental single-lap shear test load-displacement graph.
- The effect of surface treatment: the mechanical treatment of the aluminum sheets with sandpaper gave the highest shear strength after sanding for 10 s giving a 90.8% increase. In the case of chemical etching of the surface with NaOH solution, the highest value was achieved after 45-minute treatment, enhancing the shear strength by 77% in comparison to the untreated reference sample. Hence, surface treatment positively affects the strength, because it creates either holes and valleys or micropores on the surface, increasing the contact area which results in better interfacial adhesion.
- Synergistic effect: the mechanical treatment combined with CNF increased the shear strength of adhesive joints by 132% when treated for 5 seconds, and the chemical treatment - by 137% when etched for 45 minutes compared to the reference sample.

To extend the study for lap joints with nanoparticles, it is proposed to do DCB and ENF tests to get crack propagation energy failure values, as they are required to get accurate results for simulation for 0.5 - 2 wt% of nanoparticles. It is suggested to study mode 1 and mode 2 energy evaluation and numerical calculation methods. Moreover, the obtained results may be used directly in a further experimental study of multilayer FMLs.

Bibliography

[1] R. J. H. Wanhill, "GLARE®: a versatile Fibre Metal Laminate (FML) concept," in *Indian Institute of Metals series*, 2016, pp. 291–307. doi: 10.1007/978-981-10-2134-3_13.

[2] T. Sınmazçelik, E. Avcu, M. Ö. Bora, and O. Çoban, "A review: Fibre metal laminates, background, bonding types and applied test methods," *Materials in Engineering*, vol. 32, no. 7, pp. 3671–3685, Aug. 2011, doi: 10.1016/j.matdes.2011.03.011.

[3] Z. Ding, H. Wang, J. Luo, and N. Li, "A review on forming technologies of fibre metal laminates," *International Journal of Lightweight Materials and Manufacture*, vol. 4, no. 1, pp. 110–126, Mar. 2021, doi: 10.1016/j.ijlmm.2020.06.006.

[4] A. A. Khurram, R. Hussain, H. Afzal, A. Akram, and T. Subhanni, "Carbon nanotubes for enhanced interface of fiber metal laminate," *International Journal of Adhesion and Adhesives*, vol. 86, pp. 29–34, Nov. 2018, doi: 10.1016/j.ijadhadh.2018.08.008.

[5] R. Eslami-Farsani, H. Aghamohammadi, S. M. R. Khalili, H. Ebrahimnezhad-Khaljiri, and H. Jalali, "Recent trend in developing advanced fiber metal laminates reinforced with nanoparticles: A review study," *Journal of Industrial Textiles*, vol. 51, no. 5_suppl, pp. 7374S-7408S, Aug. 2020, doi: 10.1177/1528083720947106.

[6] N. Saba *et al.*, "Thermal and dynamic mechanical properties of cellulose nanofibers reinforced epoxy composites," *International Journal of Biological Macromolecules*, vol. 102, pp. 822–828, Sep. 2017, doi: 10.1016/j.ijbiomac.2017.04.074.

[7] A. Fereidoon, N. Kordani, D. D. Ganji, and M. G. Ahangari, "Effect of carbon nanotube on adhesion strength of e-Glass/Epoxy Composite and alloy Aluminum surface," *World Applied Sciences Journal*, vol. 9, pp. 204–210, 2010.

[8] N. M. Mubarak, E. C. Abdullah, N. S. Jayakumar, and J. N. Sahu, "An overview on methods for the production of carbon nanotubes," *Journal of Industrial and Engineering Chemistry/Journal of Industrial and Engineering Chemistry - Korean Society of*

Industrial and Engineering Chemistry, vol. 20, no. 4, pp. 1186–1197, Jul. 2014, doi: 10.1016/j.jiec.2013.09.001.

[9] U. Kulshrestha, T. Gupta, P. Kumawat, H. Jaiswal, S. B. Ghosh, and N. N. Sharma, "Cellulose nanofibre enabled natural rubber composites: Microstructure, curing behaviour and dynamic mechanical properties," *Polymer Testing*, vol. 90, p. 106676, Oct. 2020, doi: 10.1016/j.polymertesting.2020.106676.

[10] Q. Tarrés, Q. Tarrés, M. Alcalà, and P. Mutjé, "Research on the strengthening advantages on using cellulose nanofibers as polyvinyl alcohol reinforcement," *Polymers*, vol. 12, no. 4, p. 974, Apr. 2020, doi: 10.3390/polym12040974.

[11] K. A. Patankar, T. H. Kalantar, C. Simon, E. Nicoli, B. Tuft, and M. Crimmins, "Application of high-throughput methodologies and artificial intelligence for adhesion testing," in *Elsevier eBooks*, 2023, pp. 751–775. doi: 10.1016/b978-0-323-91214-3.00020-x.

[12] A. Redmann, V. Damodaran, F. Tischer, P. Prabhakar, and T. A. Osswald, "Evaluation of Single-Lap and block shear test methods in adhesively bonded composite joints," *Journal of Composites Science*, vol. 5, no. 1, p. 27, Jan. 2021, doi: 10.3390/jcs5010027.

[13] I. F. Villegas and C. Rans, "The dangers of single-lap shear testing in understanding polymer composite welded joints," *Philosophical Transactions - Royal Society. Mathematical, Physical and Engineering Sciences/Philosophical Transactions - Royal Society. Mathematical, Physical and Engineering Sciences*, vol. 379, no. 2203, p. 20200296, Jun. 2021, doi: 10.1098/rsta.2020.0296.

[14] A. S. Yaghoubi and B. Liaw, "Thickness influence on ballistic impact behaviors of GLARE 5 fiber-metal laminated beams: Experimental and numerical studies," *Composite Structures*, vol. 94, no. 8, pp. 2585–2598, Jul. 2012, doi: 10.1016/j.compstruct.2012.03.004.

[15] M. Kamocka and R. J. Mania, “Post-buckling response of FML column with delamination,” *Composite Structures*, vol. 230, p. 111511, Dec. 2019, doi: 10.1016/j.compstruct.2019.111511.

[16] M. Zaczynska and R. J. Mania, “Dynamic stability of thin-walled FML columns including delamination,” *Composite Structures*, vol. 290, p. 115478, Jun. 2022, doi: 10.1016/j.compstruct.2022.115478.

[17] C. T. T. Farias, E. F. S. Filho, Y. T. B. Santos, and I. S. Ribeiro, *Spectral analysis of the propagation of lamb waves on Fibre-Metal laminated plates to detect and evaluate different defects*. 2012. [Online]. Available: https://ndt.net/article/wcndt2012/papers/436_wcndtfinal00436.pdf

[18] B. Mahato, S. V. Lomov, A. Shiverskii, M. Owais, and S. G. Abaimov, “A review of Electrospun Nanofiber interleaves for interlaminar toughening of composite laminates,” *Polymers*, vol. 15, no. 6, p. 1380, Mar. 2023, doi: 10.3390/polym15061380.

[19] M. Megahed, M. a. A. El-baky, A. M. Alsaeedy, and A. E. Alshorbagy, “An experimental investigation on the effect of incorporation of different nanofillers on the mechanical characterization of fiber metal laminate,” *Composites. Part B, Engineering*, vol. 176, p. 107277, Nov. 2019, doi: 10.1016/j.compositesb.2019.107277.

[20] H. Khoramishad, H. Alikhani, and S. Dariushi, “An experimental study on the effect of adding multi-walled carbon nanotubes on high-velocity impact behavior of fiber metal laminates,” *Composite Structures*, vol. 201, pp. 561–569, Oct. 2018, doi: 10.1016/j.compstruct.2018.06.085.

[21] A. Z. Zakaria and K. Shelesh-nezhad, “Introduction of nanoclay-modified fiber metal laminates,” Engineering Fracture Mechanics, vol. 186, pp. 436–448, 2017. https://doi.org/10.1016/j.engfracmech.2017.10.023

[22] W. Wu, D. Abliz, B. Jiang, G. Ziegmann, and D. Meiners, “A novel process for cost effective manufacturing of fiber metal laminate with textile reinforced Pcbt composites and aluminum alloy,” Composite Structures, vol. 108, pp. 172–180, 2014.

[23] M. Mohamad, H. F. Marzuki, E. A. E. Ubaidillah, M. F. Z. Abidin, S. Omar, and I. M. Rozi, “Effect of Surface Roughness on Mechanical Properties of Aluminium-Carbon Laminates Composites,” Advanced Materials Research, vol. 879, pp. 51–57, 2014.

[24] A. Purnowidodo, S. S. Arief, and F. H. Iman, “Effect Surface Roughness on Fatigue Crack Propagation Behaviour of FibreMetal Laminates (FMLs),” International Journal of Automotive and Mechanical Engineering, vol. 16, pp. 6588–6604, 2019.

[25] M. M. E., H. Aghamohammadi, S. N. H. Abbandanak, G. R. Aghamirzadeh, R. Eslami-Farsani, and S. M. H. Siadati, “Effects of applying a combination of surface treatments on the mechanical behavior of basalt fiber metal laminates,” International Journal of Adhesion and Adhesives, vol. 92, pp. 133–141, 2019.

[26] M. Dro´zdziel-Jurkiewicz and J. Bienia´s, “Evaluation of Surface Treatment for Enhancing Adhesion at the Metal–Composite Interface in Fibre Metal-Laminates,” Materials, vol. 15, p. 6118, 2022.

[27] N. G. González-Canché, E. A. Flores-Johnson, P. Cortes, and J. G. Carrillo, “Evaluation of surface treatments on 5052-H32 aluminum alloy for enhancing the interfacial adhesion of thermoplastic-based fiber metal laminates,” *International Journal of Adhesion and Adhesives*, vol. 82, pp. 90–99, Apr. 2018, doi: 10.1016/j.ijadhadh.2018.01.003.

[28] N. M. Zain, S. Ahmad, and E. S. Ali, “Effect of surface treatments on the durability of green polyurethane adhesive bonded aluminium alloy,” *International Journal of Adhesion and Adhesives*, vol. 55, pp. 43–55, Dec. 2014, doi: 10.1016/j.ijadhadh.2014.07.007.

[29] E. S. Gadelmawla, M. M. Koura, T. M. A. Maksoud, I. M. Elewa, and H. Soliman, “Roughness parameters,” *Journal of Materials Processing Technology*, vol. 123, no. 1, pp. 133–145, Apr. 2002, doi: 10.1016/s0924-0136(02)00060-2.

[30] D. Castro-Casado, “Chemical treatments to enhance surface quality of FFF manufactured parts: a systematic review,” *Progress in Additive Manufacturing*, vol. 6, no. 2, pp. 307–319, Jan. 2021, doi: 10.1007/s40964-020-00163-1.

[31] N. S. Murthy, “Techniques for analyzing biomaterial surface structure, morphology and topography,” in *Elsevier eBooks*, 2011, pp. 232–255. doi: 10.1533/9780857090768.2.232.

[32] B. Jagadeesh, M. Duraiselvam, A. Bera, and A. Arya, “Effect of laser micromachining and laser shock peening on the performance of Inconel alloy parts for aerospace application,” in *Elsevier eBooks*, 2023. doi: 10.1016/b978-0-323-96020-5.00124-2.

[33] G. Mitaľ, J. Dobránsky, J. Ružbarský, and Š. Olejárová, “Application of laser profilometry to evaluation of the surface of the workpiece machined by abrasive waterjet technology,” *Applied Sciences*, vol. 9, no. 10, p. 2134, May 2019, doi: 10.3390/app9102134.

[34] X. Wu, L. Zhan, X. Zhao, X. Wang, and T. Chang, “Effects of surface pre-treatment and adhesive quantity on interface characteristics of fiber metal laminates,” *Composite Interfaces*, vol. 27, no. 9, pp. 829–843, Dec. 2019, doi: 10.1080/09276440.2019.1707023.

[35] L. Guo, J. Liu, H. Xia, X. Li, X. Zhang, and H. Yang, “Effects of surface treatment and adhesive thickness on the shear strength of precision bonded joints,” *Polymer Testing*, vol. 94, p. 107063, Feb. 2021, doi: 10.1016/j.polymertesting.2021.107063.

[36] S. Laurén, “How to utilize contact angles in surface characterization: Roughness corrected contact angle,” Biolin Scientific, https://www.biolinscientific.com/blog/how-to-utilize-contact-angles-in-surface-characterization-roughness-corrected-contact-angle (accessed Apr. 24, 2024). T. M. S. Faneco, R. D. S. G. Campilho, F. Silva, and R.

[37] Lopes, “Strength and fracture characterization of a novel polyurethane adhesive for the automotive industry,” *Journal of Testing and Evaluation*, vol. 45, no. 2, p. 20150335, Feb. 2016, doi: 10.1520/jte20150335.

[38] J. M. D. Teixeira, R. D. S. G. Campilho, and F. Silva, “Numerical assessment of the Double-Cantilever Beam and Tapered Double-Cantilever Beam tests for the GIC determination of adhesive layers,” *the Journal of Adhesion/Journal of Adhesion*, vol. 94, no. 11, pp. 951–973, Feb. 2018, doi: 10.1080/00218464.2017.1383905.

[39] A. Arrese, N. Carbajal, G. Vargas, and F. Mujika, “A new method for determining mode II R-curve by the End-Notched Flexure test,” *Engineering Fracture Mechanics*, vol. 77, no. 1, pp. 51–70, Jan. 2010, doi: 10.1016/j.engfracmech.2009.09.008.

[40] M. F. S. F. De Moura, “Numerical simulation of the ENF test for the mode-II fracture characterization of bonded joints,” *Journal of Adhesion Science and Technology*, vol. 20, no. 1, pp. 37–52, Jan. 2006, doi: 10.1163/156856106775212422.

[41] F. G. A. Silva, J. J. L. Morais, N. Dourado, J. Xavier, F. A. M. Pereira, and M. F. S. F. De Moura, “Determination of cohesive laws in wood bonded joints under mode II loading using the ENF test,” *International Journal of Adhesion and Adhesives*, vol. 51, pp. 54–61, Jun. 2014, doi: 10.1016/j.ijadhadh.2014.02.007.

[42] G. P. Anderson, K. L. DeVries, and G. Sharon, “Evaluation of adhesive test methods,” in *Springer eBooks*, 1984, pp. 269–287. doi: 10.1007/978-1-4613-2749-3_18.

[43] T. Sinmazcelik, E. Avcu, M. O. Bora, and O. Coban, “A review: Fibre metal laminates, background, bonding types and applied test methods,” Materials & Design, vol. 32, pp. 3671–3685, 2011.

[44] Z. Ding, H. Wang, J. Luo, and N. Li, “A review on forming technologies of fibre metal laminates,” International Journal of Lightweight Materials and Manufacture, vol. 4, pp. 110–126, 2021.

[45] A. A. Khurram, R. Hussain, H. Afzal, A. Akram, and T. Subhanni, “Carbon nanotubes for enhanced interface of fiber metal laminate,” International Journal of Adhesion and Adhesives, vol. 86, pp. 29–34, 2018.

[46] N. Saba, A. Safwan, M. L. Sanyang, F. Mohammad, M. Pervaiz, M. Jawaid, O. Y. Alothman, and M. Sain, “Thermal and dynamic mechanical properties of cellulose nanofibers reinforced epoxy composites ,” International Journal of Biological Macromolecules, vol. 102, pp. 822–828, 2017.

[47] R. Eslami-Farsani, H. Aghamohammadi, S. M. Khalili, H. Ebrahimnezhad-Khaljiri, and H. Jalali, “Recent trend in developing advanced fiber metal laminates reinforced with nanoparticles: A review study,” Journal of Industrial Textiles, vol. 51, 2020.

[48] A. Fereidoon, N. Kordani, D. D. Ganji, and M. G. Ahangari, “Effect of carbon nanotube on adhesion strength of e-Glass/Epoxy Composite and alloy Aluminum surface,” World Applied Sciences Journal, vol. 9, pp. 204–210, 2010.

[49] N. M. Mubarak, E. C. Abdullah, N. S. Jayakumar, and J. N. Sahu, “An overview on methods for the production of carbon nanotubes,” Journal of Industrial and Engineering Chemistry, vol. 20, pp. 1186–1197, 2014.

[50] U. Kulshrestha, T. Gupta, P. Kumawat, H. Jaiswal, S. B. Ghosh, and N. N. Sharma, “Cellulose nanofibre enabled natural rubber composites: Microstructure, curing behaviour and dynamic mechanical properties,” Polymer Testing, vol. 90, p. 106676, 2020.

[51] K. A. Patankar, T. Kalantar, S. Cook, E. Nikoli, B. Tuft, and M. Crimmins, “Application of high-throughput methodologies and artificial intelligence for adhesion testing,” Advances in Structural Adhesive Bonding (Second Edition), vol. 22, pp. 751–775, 2023.

[52] K. V. Redmann, A. I. Ginnis, C. G. Politis, and P. D. Kaklis, “Evaluation of Single-Lap and Block Shear Test Methods in Adhesively Bonded Composite Joints,” Journal of Composites Science, vol. 5, p. 27, 2021.

[53] I. F. Villegas and C. Rans, “The dangers of single-lap shear testing in understanding polymer composite welded joints,” Philosophical Transactions of the Royal Society A: Mathematical, Physical and Engineering Sciences, vol. 379, 2021.

[54] M. Megahed, M. A. Abd El-baky, A. M. Alsaeedy, and A. Alshorbagy, “An experimental investigation on the effect of incorporation of different nanofillers on the mechanical characterization of fiber metal laminate,” Composites Part B: Engineering, vol. 176, p. 107277, 2019.

[55] H. Khoramishad, H. Alikhani, and S. Dariushi, “An experimental study on the effect of adding multi-walled carbon nanotubes on high-velocity impact behavior of fiber metal laminates,” Composite Structures, vol. 201, pp. 561–569, 2018.

[56] A. Z. Zakaria and K. Shelesh-nezhad, “Introduction of nanoclay-modified fiber metal laminates,” Engineering Fracture Mechanics, vol. 186, pp. 436–448, 2017.

[57] W. Wu, D. Abliz, B. Jiang, G. Ziegmann, and D. Meiners, “A novel process for cost effective manufacturing of fiber metal laminate with textile reinforced Pcbt composites and aluminum alloy,” Composite Structures, vol. 108, pp. 172–180, 2014.

[58] M. Mohamad, H. F. Marzuki, E. A. E. Ubaidillah, M. F. Z. Abidin, S. Omar, and I. M. Rozi, “Effect of Surface Roughness on Mechanical Properties of Aluminium-Carbon Laminates Composites,” Advanced Materials Research, vol. 879, pp. 51–57, 2014.

[59] A. Purnowidodo, S. S. Arief, and F. H. Iman, “Effect Surface Roughness on Fatigue Crack Propagation Behaviour of FibreMetal Laminates (FMLs),” International Journal of Automotive and Mechanical Engineering, vol. 16, pp. 6588–6604, 2019.

[60] M. M. E., H. Aghamohammadi, S. N. H. Abbandanak, G. R. Aghamirzadeh, R. Eslami-Farsani, and S. M. H. Siadati, “Effects of applying a combination of surface treatments on the mechanical behavior of basalt fiber metal laminates,” International Journal of Adhesion and Adhesives, vol. 92, pp. 133–141, 2019.

[61] M. Dro´zdziel-Jurkiewicz and J. Bienia´s, “Evaluation of Surface Treatment for Enhancing Adhesion at the Metal–Composite Interface in Fibre Metal-Laminates,” Materials, vol. 15, p. 6118, 2022.

[62] E. E. Gadelmawla, M. M. Koura, T. M. A. Maksoud, I. M. Elewa, and H. H. Soliman, “Roughness parameters,” Journal of Materials Processing Technology, vol. 123, pp. 133–145, 2002.

[63] N. Murthy, “Techniques for analyzing biomaterial surface structure, morphology and topography,” Surface Modification of Biomaterials, vol. 9, pp. 232–255, 2011.

[64] B. Jagadeesh, M. Duraiselvam, A. Bera, and A. Arya, “Effect of laser micromachining and laser shock peening on the performance of Inconel alloy parts for aerospace application,” Reference Module in Materials Science and Materials Engineering, 2023.

[65] G. Mital’, J. Dobransky, J. Ruzbarsky, and S. Olejarova, “Application of Laser Profilometry to Evaluation of the Surface of the Workpiece Machined by Abrasive Waterjet Technology,” Applied Sciences, vol. 9, p. 2134, 2019.

[66] T. M. Faneco, R. D. Campilho, F. J. Silva, and R. M. Lopes, “Strength and Fracture Characterization of a Novel Polyurethane Adhesive for the Automotive Industry,” Journal of Testing and Evaluation, vol. 45, p. 20150335, 2016.

[67] J. Teixeira, R. Campilho, and F. da Silva, “Numerical assessment of the Double-Cantilever Beam and Tapered Double-Cantilever Beam tests for the GIC determination of adhesive layers,” The Journal of Adhesion, vol. 94, pp. 951–973, 2018.

[68] A. Arrese, N. Carbajal, G. Vargas, and F. Mujika, “A new method for determining mode II R-curve by the end-notched flexure test,” Engineering Fracture Mechanics, vol. 77, pp. 51–70, 2010.

[69] M. F. Moura, “Numerical simulation of the ENF test for the mode-II fracture characterization of bonded joints,” Journal of Adhesion Science and Technology, vol. 20, pp. 37–52, 2006.

[70] F. G. A. Silva, J. J. L. Morais, N. Dourado, J. Xavier, F. A. M. Pereira, and M. F. S. F. de Moura, “Determination of cohesive laws in wood bonded joints under mode II loading using the ENF test,” International Journal of Adhesion and Adhesives, vol. 51, pp. 54–61, 2014.

[71] G. P. Anderson, K. L. DeVries, and G. Sharon, “Evaluation of adhesive test methods,” Adhesive Joints, pp. 269–287, 1984.

[72] S. Bayramoglu, S. Akpinar, and A. Çalık, “Numerical Analysis of elasto-plastic adhesively single step lap joints with cohesive zone models and its experimental verification,” Journal of Mechanical Science and Technology, vol. 35, pp. 641–649, 2021.

[73] K. V. Boutar, A. I. Ginnis, C. G. Politis, and P. D. Kaklis, “A Study of the Interlaminar Fracture Toughness of Unidirectional Flax/Epoxy Composites,” Computer Methods in Applied Mechanics and Engineering, vol. 4, p. 66, 2017.

[74] M. N. F. E. a. Norrrahim, “Performance evaluation of cellulose nanofiber reinforced polymer composites,” Functional Composites and Structures, vol. 3, p. 024001, 2021.

[75] F. Narita, Y. Wang, H. Kurita, and M. Suzuki, “Multi-Scale Analysis and Testing of Tensile Behavior in Polymers with Randomly Oriented and Agglomerated Cellulose Nanofibers,” Special Issue Advanced Mechanical Modeling of Nanomaterials and Nanostructures, vol. 10, p. 700, 2020.

[76] A. Venugopal and E. Sudhagar P, “Enhancing shear and flexural strength of single lap composite joints with a graphene nanoparticle-reinforced adhesive through a co-curing technique,” Polymer Composites, vol. 45, no. 5, pp. 4202–4220, Dec. 2023. doi:10.1002/pc.28053

[77] P. J. Charitidis, “The effect of nanoparticles in single lap joints studied by numerical analyses,” European Journal of Engineering Research and Science, vol. 5, no. 10, pp. 1288–1293, Oct. 2020. doi:10.24018/ejers.2020.5.10.2194

[78] E. V. Prasad, C. Sivateja, and S. K. Sahu, “Effect of nanoalumina on fatigue characteristics of fiber metal laminates,” Polymer Testing, vol. 85, p. 106441, May 2020. doi:10.1016/j.polymertesting.2020.106441

[79] F. Bahari-Sambran, J. Meuchelboeck, E. Kazemi-Khasragh, R. Eslami-Farsani, and S. Arbab Chirani, “The effect of surface modified nanoclay on the interfacial and mechanical properties of basalt fiber metal laminates,” Thin-Walled Structures, vol. 144, p. 106343, Nov. 2019. doi:10.1016/j.tws.2019.106343

[80] M. H. Khan, O. A. Gali, A. Edrisy, and A. R. Riahi, “Effect of oxidation and surface roughness on the shear strength of single-lap-joint adhesively bonded metal specimens by tension loading,” Applied Adhesion Science, vol. 4, no. 1, Dec. 2016. doi:10.1186/s40563-016-0077-1

[81] X. Xu, F. Liu, L. Jiang, J. Zhu, D. M. Haagenson, and D. P. Wiesenborn, “Cellulose Nanocrystals vs. Cellulose Nanofibrils: A Comparative Study on Their Microstructures and Effects as Polymer Reinforcing Agents,” ACS Applied Materials & Interfaces, vol. 5, no. 8, pp. 2999–3009, Apr. 2013, doi: 10.1021/am302624t.

[82] M. Fazeli and R. A. Simão, “The effect of cellulose nanofibers on the properties of starch biopolymer,” Macromolecular Symposia, vol. 380, no. 1, Aug. 2018, doi: 10.1002/masy.201800110.

[83] S. Noormohammed, D. Sarkar, R. W. Paynter, D. Gallant, and M. Eskandarian, “A simple surface treatment and characterization of AA 6061 aluminum alloy surface for adhesive bonding applications,” Applied Surface Science, vol. 261, pp. 742–748, Nov. 2012, doi: 10.1016/j.apsusc.2012.08.091.

[84] Y. Hu, B. Yuan, F. Cheng, and X. Hu, “NaOH etching and resin pre-coating treatments for stronger adhesive bonding between CFRP and aluminium alloy,” Composites. Part B, Engineering, vol. 178, p. 107478, Dec. 2019, doi: 10.1016/j.compositesb.2019.107478.

[85] M. I. Shahid and S. A. Hashim, “Effect of surface roughness on the strength of cleavage joints,” International Journal of Adhesion and Adhesives, vol. 22, no. 3, pp. 235–244, Jan. 2002, doi: 10.1016/s0143-7496(01)00059-8.

[86] X. Wu et al., “Synergistic delamination toughening of glass Fiber-Aluminum laminates by surface treatment and graphene oxide interleaf,” Nanoscale Research Letters, vol. 15, no. 1, Apr. 2020, doi: 10.1186/s11671-020-03306-z.

[87] R. D. S. G. Campilho, M. D. Banea, A. M. G. Pinto, L. F. M. da Silva, and A. M. P. de Jesus, “Strength prediction of single- and double-lap joints by standard and extended finite element modelling,” International Journal of Adhesion and Adhesives, vol. 31, no. 5, pp. 363–372, Jul. 2011. doi:10.1016/j.ijadhadh.2010.09.008

[88] M. Z. Sadeghi et al., “Failure load prediction of adhesively bonded single lap joints by using various FEM techniques,” International Journal of Adhesion and Adhesives, vol. 97, p. 102493, Mar. 2020. doi:10.1016/j.ijadhadh.2019.102493

[89] A. M. Pinto, A. G. Magalhães, R. D. Campilho, M. F. de Moura, and A. P. Baptista, “Single-lap joints of similar and dissimilar adherends bonded with an acrylic adhesive,” The Journal of Adhesion, vol. 85, no. 6, pp. 351–376, May 2009. doi:10.1080/00218460902880313